Ran Xiao

Numerical investigation for the moment caused by shallow water sloshing under a transient roll motion

School of Engineering

Thesis submitted for examination for the degree of Master of Science in Technology.

Espoo 04.09.2015

Thesis supervisor:

Prof. Pentti Kujala

co-supervisor: Prof. Marilena Greco(NTNU)

Thesis advisor:

M.Sc. (Tech.) Teemu Manderbacka

Aalto University
School of Engineering

AALTO UNIVERSITY
SCHOOL OF ENGINEERING

ABSTRACT OF THE
MASTER'S THESIS

Author: Ran Xiao

Title: Numerical investigation for the moment caused by shallow water sloshing under a transient roll motion

Date: 04.09.2015 Language: English Number of pages: 8+64

Department of Applied Mechanics

Professorship: Professor

Supervisor: Prof. Pentti Kujala & Prof. Marilena Greco (NTNU)

Advisor: M.Sc. (Tech.) Teemu Manderbacka

This paper aims to study the damping effect of the shallow water sloshing on the rectangular tank under a free decaying roll motion in 2 dimensional condition. OpenFOAM software as a CFD method is applied, and its solver interDyMFoam is used to simulate the sloshing phenomenon and process the data. A good representation of the fluid motion evolution and a sound evaluation of the sloshing moment history are given.

My sloshing case is a 2D rectangular tank with the filling ratio of 0.012, starting with an initial heeling angle of 8.151 degrees, and the simulated time span is 7 seconds when the first two impacts have taken place. The obtained simulation sloshing moments are compared with the quasi-static moment, while an image comparison is also conducted between the tank test images and the simulation animation to validate the simulation.

The damping effect on the tank is studied in time domain. The sloshing moment does not always dampen the tank motion. And it gradually catches up with the quasi-static moment in term of time, while its amplitude decays along with the tank motion. The simulated water motion is satisfactory in general with limited unphysical phenomena. Understanding and experience of interDyMFoam throughout the usage are shared. Consequently, the thesis offers a both qualitatively and quantitatively good study on the shallow water sloshing in transient excitation motion.

Keywords: Shallow water sloshing; Transient tank motion; Damping effect; CFD; OpenFOAM;

Preface

This paper is my master thesis, as a part of my study at Applied Department at Aalto University and at the faculty of Marine Technology at Norwegian University of Science and Technology.

Firstly I really feel so grateful that I could have a chance being here, living here and studying here. For this thesis, I have to thank Professor Pentti Kujala. Without his help, I would not be able to find this thesis work and have it done here at Aalto University. He is a very energetic and friendly senior, loving playing jokes with some his accent. I sincerely appreciate for all he did for me.

Then I would like to mention my dear advisor and my colleagues, dear Mr. Teemu Manderbacka, respectful Mr. Tommi Mikkola and lovely Mr. Otto Puolakka.

To Teemu, all I have is endless gratitude. As my advisor, he helped with all he can do, more than what an advisor is responsible for. Sometimes I just felt bad for my knowledge since my background does not so concentrate on hydrodynamics. But he always had patience and faith with me, teaching me quite a lot of knowledge that I maybe should have known. And he was also very strict with my work, giving lots of comments and invaluable criticism on my work so that I have to refine it again and again and becomes better and better. Oh man, Teemu, you are such a friendly advisor and nice friend. Kiitos, for everything.

To Mr. Mikkola, I have to say he is my major source of CFD knowledge and a unmarked reference in my thesis. Also I need to say kitos for his incredible patience while helping me with OpenFOAM. I think I had troubled him for maybe 1000000 times for my questions. He always sat down, well sometimes he stood, and gave me detailed answers for my countless 'why'. He always acted like a kind and humorous friend to us, and I really appreciate it. Thank you.

To Otto, It is my fortune to have you sitting behind me. You helped me so much and taught me many trivial but also helpful thing. And when I really felt upset by my simulation, I looked back, and probably I could find you and your upset simulation, which, I have to say, made me feel a lot better. I am so sorry about that, and, thank you.

Lastly, I couldn't have been here without the help and support from my family, especially my mom, and my friends. I would like to give you a big embrace. Xie xie ni men.

Otaniemi, 04.09.2015

Ran Xiao

Contents

Symbols and abbreviations

Symbols

A	area of the control volume surface
B	tank width
b	length of wet tank bottom
$cAlpha$	the coefficient to compress the interface in VOF method
D	tank length in x direction
dL	length of a virtual cut on the fluid surface
F	volume fraction
g	gravity acceleration
h/B	filling ratio
h	water depth in the tank
$h*$	average height of the sloshing water
i	numbers of surfaces of the control volume
L	characteristic length
m_{water}	mass of the flooding water in tank
$\bar{n}$	the unit vector normal to the control volume surface
n	a positive integer
P	the control volume of interest
p	pressure
$p_{hydrostatic}$	hydrostatic pressure
RAO	amplitude of roll divided by effective maximum wave slope
Re	Reynolds Number
T_1	lowest natural frequency of the sloshing fluid
T_n	eigenfrequency of the sloshing fluid
t	time
u	velocity in x direction
U	the velocity of fluid
$\mathbf{u}$	fluid total velocity in RANS equations
$\mathbf{U}$	mean term in fluid total velocity in RANS equations
u'	fluctuation term in fluid total velocity in RANS equations
U_∞	fluid velocity at far field
U_e	fluid velocity exists along the body surface
v	velocity in y direction
$\triangle V$	volume of the control volume
V	fluid velocity when considering RANS equations
V_0	sloshing water volume
$\vec{v_w}$	water velocity
$\vec{v_a}$	air velocity
$\vec{v_{r\alpha}}$	relative velocity at the interface between the two phases
w	velocity in z direction
We	Weber number
W, E, N, S	directions correspond to west, east, north and south
x	displacement in x direction
y	displacement in y direction
z	displacement in z direction

Symbols

$\frac{K_{ta}}{\rho g l^3 L_t}$	the nondimensional sloshing moment amplitude
$\sigma(l/g)^{\frac{1}{2}}$	nondimensional frequency of the tank motion
ε_t	phase lag between the tank motion and the sloshing moment
ρ	density
Υ	coefficient of surface tension
ν	kinematic viscosity
θ	tank roll angle
η_4,	displacement of roll
η_{4a}	amplitude of roll
ϕ	variables of fluid of interest include velocity and pressure
τ	shear stress in boundary layer
μ	dynamic viscosity
$\varphi(t)$	physical properties in RANS equations
Φ	mean term in RANS equations
$\varphi'(t)$	fluctuation term in RANS equations
μ_t	eddy viscosity
ω_e	tuning factor, ratio between excitation frequency and fluid natural frequency
ω_t	stabilizer tuning factor, ratio of ship natural frequency to fluid natural frequency
RAO	amplitude of roll divided by effective maximum wave slope

Operators

∇	Nabla operator
$\frac{\mathrm{d}}{\mathrm{d}t}$	derivative with respect to variable t
$\frac{\partial}{\partial t}$	partial derivative with respect to variable t
$\sum_i$	sum over index i
$grad(\mathbf{A})$	gradient of A
$div(\mathbf{A})$	divergence of A
Δ	difference or change in a certain quantity

Abbreviations

2D	two-dimensional
3D	three-dimensional
BC	boundary condition
BEM	Boundary Element Method
CFD	computational fluid dynamics
CV	control volume
CoG	Center of Gravity
FVM	finite volume method
FDM	finite difference method
LS	Level Set
NS	Navier-Stokes
RANS	Reynolds-averaged Navier-Stokes
SPH	Smoothed Particle Hydrodynamics
VOF	volume of fluid

1 Introduction

1.1 Motivation

Along with the development of shipbuilding, ships and offshore structures are growing more gigantic and complex ever. In the meanwhile, safety is also more and more emphasized by the regulations and the market. Any safety flaw of ship design may trigger a disaster on the sea, costing millions of dollars and losing invaluable lives. People try to avoid tragedies like Titanic, but shipwreck can still be seen on the newspaper nowadays. For maritime engineering, safety is always a fundamentally critical topic, and naval architecture safety involves quite many aspects, among which an important one is stability. Sufficient stability guarantees that the ship is able to survive from violent sea states and recover from certain enforced motion or heeling caused by winds, waves and so on. To secure enough stability while design, liquid with free surface on board is an essential factor that needs to be taken into account, because sloshing phenomenon will probably be excited due to the ship motion and it can have a significant effect on ship stability.

Sloshing is the fluid motion within the partially filled tank or compartment in certain motion. The sloshing water exerts an extra moment coupling with the ship motion, affecting the ship stability. Transport ships carrying liquid cargo will face this issue. Besides, for ships that get damaged because of collision or grounding, they also need to deal with sloshing problem. Among all the sloshing situations, shallow water sloshing is very distinctive with other higher filling level condition, and it is a subject that is not studied so often but also matters in certain cases. In shallow water condition, when the excitation frequency is around the natural frequency of the fluid, a hydraulic jump or bore, which travels back and forth in the tank, is formed. When the steep front of the bore hits the tank wall, an impact could happen and run-up can occur along the wall. In other conditions with higher filling ratio h/B between water depth h and tank width B, the free surface motion resembles a standing wave[16]. For small ships, ingress of water through the openings on board can result in shallow water condition, and damaged ship with limited amount of water flooding in will also possibly encounter this situation. In such cases, the sloshing effect might be crucial.

The sloshing effect is tightly related with the filling ratio h/B. The ratio can greatly influence the natural frequency of the fluid which is the lowest eigenfrequency of sloshing fluid. Considering sloshing problem in frequency domain, let us assume the excitation from the tank is harmonic roll motion. Due to inertia, the fluid motion always lags behind the tank motion in term of phase. Because of the phase lag, the free surface fluid is able to exert a moment to dampen the excitation motion or increase it. The phase lag between the tank motion and the sloshing moment depends on the difference between the excitation frequency and fluid natural frequency. An example is the tank test by Vugts[21] illustrated by figure 1 where $\sigma_1(l/g)^{\frac{1}{2}}$ is the nondimensional frequency of the tank motion, ε_t marks the phase lag and l denotes the tank width only in this case of Vugts. As shown in figure 1, when the tank frequency approaches the natural frequency, the phase lag is $\pi/2$, and the sloshing moment damps the excitation with maximum amplitude due to resonance. When

excitation frequency draws away from the natural frequency, the sloshing moment amplitude gradually becomes insignificant, but the phase lag also changes accordingly at the same time, which may lead to a significant roll moment acting on the ship. Thus, in the oscillation condition that the excitation frequency doest not coincide with natural frequency, sloshing can probably bring significant instability to the ship, and this will be further elaborated in next chapter. Specifically, when the tank frequency comes close to zero, which meaning the tank moves extremely slowly, and the free surface can be considered horizontal plane, the free-surface effect starts to matter, and the fluid can exert a significant heeling moment. The heeling moment is produced by the inclination of the liquid surface and the displacement of gravity center of the fluid, and it brings instability to ships[2]. The condition that excitation frequency is near zero is called quasi-static conditin and it is almost impossible in reality. However, it is important to calculate the static stability of ships. In reality, typically the ship sails on the sea, interacting with irregular waves, currents, internal flooding water and so on, which may lead to transient ship motion. Therefore, the tank motion in this sense should be seen as transient but not harmonic, and the sloshing problem needs to be studied in time domain instead of frequency domain since there is no specific frequency of the tank motion.

Inherently, sloshing is difficult to predict theoretically because it is a highly nonlinear phenomenon with complex fluid motions such as wave breaking and mixture of air and water[16]. These phenomena are often observed in shallow water condition. To study sloshing problem, apart from analytical methods and experimental methods, numerical methods are widely applied in research. So far, some analytical solutions have been developed for the eigenfrequency of fluid under specific conditions, e.g. for rectangular fluid shape and wedge shape by Faltinsen[4]. And specifically, for shallow water sloshing with the filling ratio below 0.1, there is also analytical solution available, given by Verhagen and van Wijngaarden[19]. But due to the assumptions that are made as prerequisites, e.g. the shape of water should always be rectangular or wedge and the tank motion is harmonic, these analytical solutions are not applicable in some practical cases. Experimental study has been proved as a reliable method, but it is always expensive and time-costly. It pushes people seeking for possible alternatives. Numerical simulation is very promising in this field. It can provide with considerably good results with much less expense. Now people are trying to simplify the numerical calculation for more efficient simulation. Specifically, a method called Lumped mass method[14] is now studied to calculate the damping effect of sloshing on damaged and flooded ships in a transient motion. This method assumes the surface of sloshing water is always flat and moving with a inclining angle which is a function of the tank roll angle. The results show good agreement with the tank test except for certain shallow water cases. The significant deviation of the sloshing moment prediction in the exceptional cases concentrate around the first period of the roll motion. Hence, simulating and investigating one of these specific shallow water cases could be helpful to improve and further develop Lump Mass method[14]. Meanwhile, it is rewarding to learn the shallow water sloshing in a transient tank motion, helping us to better understand the effect by water flooding on ship stability in time domain and to secure the safety, especially for small ships and damaged

ships.

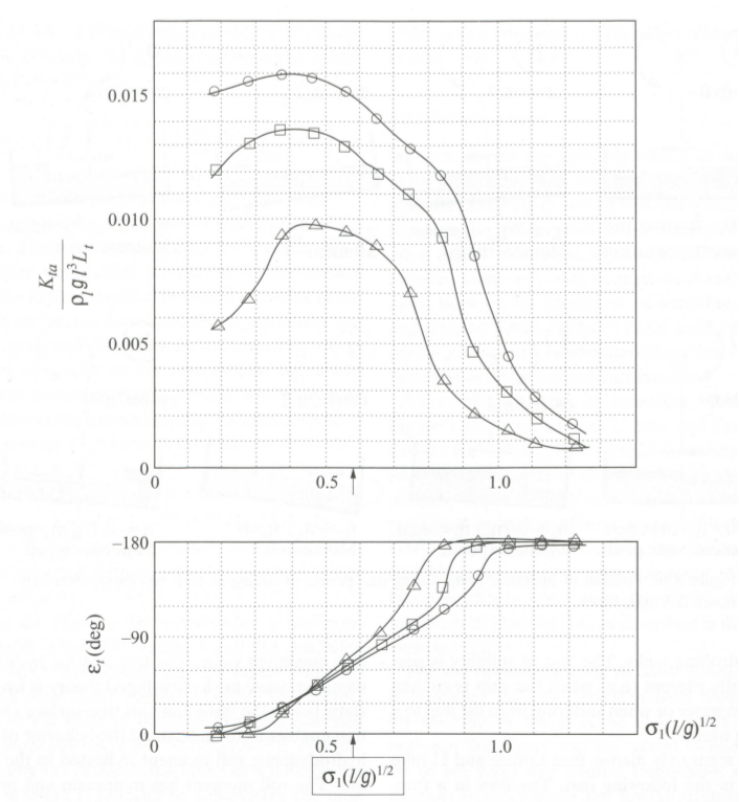

Figure 1: Relationship between the frequency difference and phase lag based on experiment[21]. The line with triangle represents amplitude of the forced tank roll motion is 0.1, while the square means amplitude as 0.0667 and the circle is 0.0333. The fluid natrual frequency is 0.59 in this case. $\frac{K_{ta}}{\rho g l^3 L_t}$ represent the nondimensional sloshing moment amplitude.

1.2 Objectives

In the thesis, I will simulate and study a specific shallow water sloshing case in transient motion with filling ratio of 0.012 using OpenFOAM, which is based on the tank test in the work[14]. The focus is on the sloshing moment prediction and damping effect on the tank motion. The paper[14] studies the sloshing moment acting on a flooding tank of a damaged ship on the sea, and the tank motion is free decaying roll motion. But in my simulation, the tank motion is a forced transient roll motion. The reason is that it is too difficult to consider all the interaction among external water, inflow effect, ship collision and so on in the simulation. It would require too much computational resources and time. To simplify the simulation, these factors are removed, while a forced transient motion is applied, which is a 'free decaying' motion recorded from the tank experiment, which will be specified in next chapter. Since my goal is to simulate the sloshing and its effect in such a tank motion but not to represent the tank motion, thus this way offers the availability to simulate

exactly the same sloshing case while it skips much potential technical difficulty.

Furthermore, the simulated sloshing evolution process will be compared with the tank test images. The point is to see how close the simulation could be to the tank test in order to ensure the simulation result is physical and valid enough. The settings of simulations will also be changed according to the problems that may take place to refine simulation quality.

To study shallow water sloshing and its damping effect, I will then compare the simulation results with quasi-static moment history. Quasi-static method is often used to study flooding effect and static stability. It is exactly in phase with the tank motion. Such a comparison can help analyse and understand the damping effect and lag between the tank motion and the simulated sloshing moment in this case.

1.3 Thesis structure

In the next section, a general theory background of sloshing follows, specifically, the shallow water condition will be explained. Then I will explain more details of the simplifications in the simulation. Reasons will be presented for why external water and other effects are omitted. Finally, an introduction of CFD about what it involves and how it works will be elaborated.

In the third section, a detailed explanation for the methods and knowledge that I will apply in the study will be presented, which includes CFD methods and theory as well as fluid mechanics. The software I apply is OpenFOAM, and a series of iterative simulation tests will be conducted. There will be a specific description for the simulation grid setup and model settings in this part.

The fourth section is where the simulation process and result are laid, including the mesh convergence test and some trials to improve the simulation. The sloshing moment histories of different cases will be plotted there, and they will be compared with the quasi-static moment as well as the tank roll motion. Besides, a detailed comparison between the simulation animation and the tank test images will be presented. The focus is on the fluid motion during the first impact and soon afterwards. According to the comparison, some initial analysis and general conclusions will be made to help link the simulation series in a logic sequence.

In the fifth section, a comprehensive analysis shall be done. The summary for the key findings and evaluation for the simulated results will be given. Some experience as well as suggestions learned throughout the simulation will be shared for the further development.

2 Background

2.1 Sloshing & damping effect

To better understand sloshing phenomenon, it is easier to start with harmonic steady state condition of the tank motion, which is more regular and in order. In this condition, the tank motion is harmonic rolling or swaying. According to Faltinsen and Timokha[4], assumption of potential flow theory is applied to simplify the sloshing phenomenon. It is proved that there are infinite eigenfrequencies and eigenmodes existing. However, only the first which is also the lowest eigenfrequency is defined as the natural frequency. As can be seen in figure 2, because the first one has the longest wave length according to the relationship $n\lambda = 2B$[4] where λ is the wavelength and n is a positive integer, the longest wave length can give the possibly largest moment and force among all the eigenmodes. In comparison, the rest eigenfrequencies are less significant. Now, by analytical study, people have found a few solutions of eigenperiods of certain cases, which include the case of 2-dimension rectangular tank. The expression for the natural periods is:[4]

$$T_n = \frac{2\pi}{\sqrt{\frac{\pi \cdot n}{B} g \cdot \tanh(\frac{\pi \cdot n}{B} h)}} \tag{1}$$

with g as gravity constant and h as water depth. The higher n is, the shorter T_n is. Often, it is classified that $h/B < 0.1$ as shallow water, h/B between 0.1 to 0.25 as intermediate and from 0.25 to 1.0 as finite liquid depth. Because the water depth is small relative to B in shallow water conditions, approximation that $h/B \to 0$ is applied, so we have $\tanh(\pi h/B) \approx \pi h/B$ and can yield equation 2. [4]

$$T_1 = 2B/\sqrt{gh} \tag{2}$$

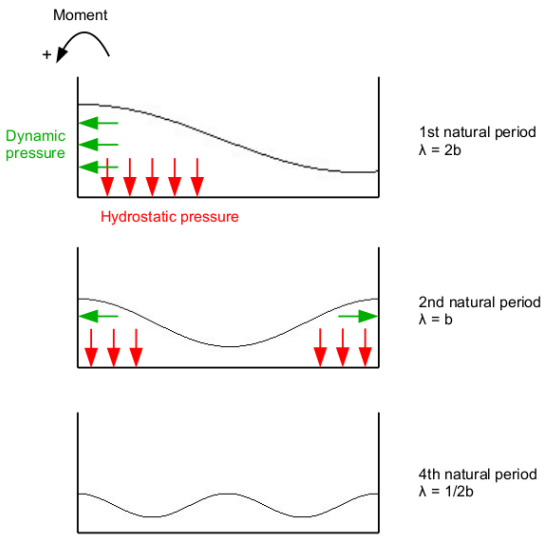

Figure 2: Eigenperiods of sloshing in rectangular [3]

Equations 1 and 2 are only applicable when the fluid domain is rectangular. In my case, as the water depth is very limited, the fluid shape in tank varies between wedge and rectangle frequently during sloshing. Thus it is not proper to consider the fluid domain as a constantly identical shape to calculate its properties such as natural frequency. Meanwhile, since the tank motion is transient, both of the periods of the tank and sloshing water vary constantly non-linearly. There will not be any significant resonance in my simulation. Therefore, this case should be studied in time domain rather than in frequency domain.

Back to the harmonic steady state condition, due to the motion of the tank, the liquid inside moves correspondingly from side to side, and there is a constant phase lag between the tank motion and sloshing moment. When the lag is around $\pi/2$, sloshing moment counteracts the tank motion in its entire period with maximum amplitude. This can be illustrated in figure 4. And in figure 3, the change of roll motion amplitude of the ships with and without a stabilizer along with the change of excitation frequency is presented. It shows what happens to the ship stability with change of tuning factor $\hat{\omega_e}$ which is the ratio between the excitation frequency acting on the ship and the fluid natural frequency. RAO is the amplitude of roll divided by effective maximum wave slope. The stabilizer tuning factor ω_t is equal to 1.08 in figure 3, which is the ratio between the ship natural frequency and fluid natural frequency. Therefore, the ship almost resonates while the fluid resonates. The figure clearly shows that under resonance, the stability difference between the ships with a stabilizer and without is very noticeable when $\hat{\omega_e}$ is near 1.0. While $\hat{\omega_e}$ is out of the vicinity of 1.0, the effect of sloshing moment becomes insignificant.

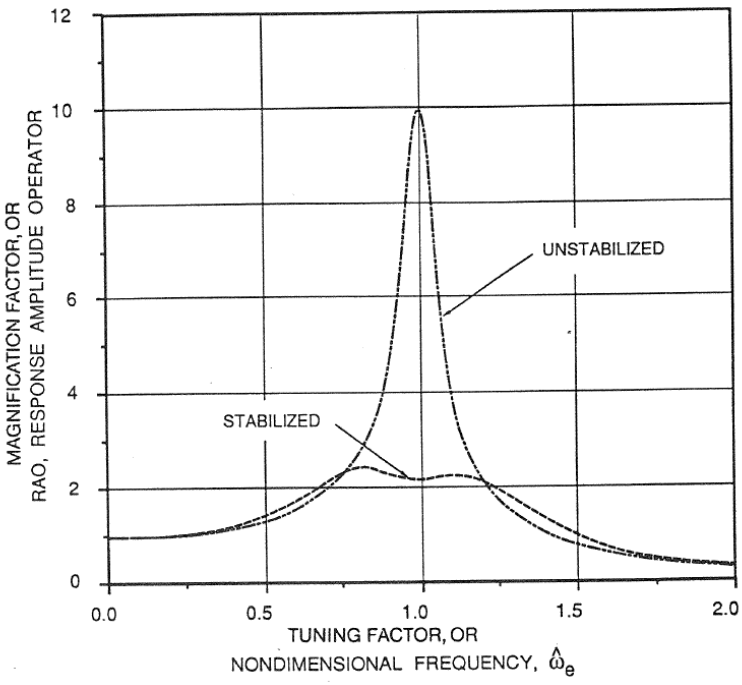

Figure 3: Effect of stabilizer, namely the tank, on the ship stability[11].

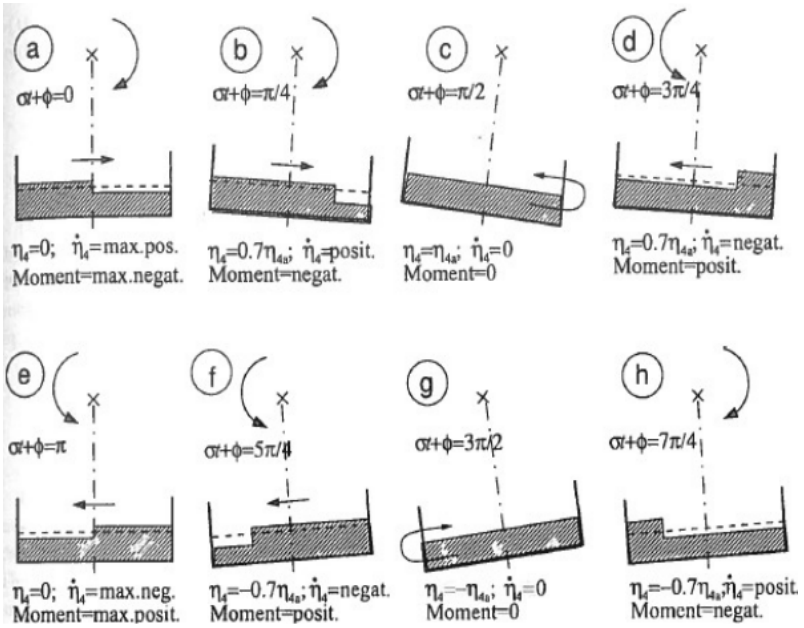

Figure 4: Sloshing water motion in the tank when phase lage is $\pi/2$[4]. η_4 is the excitation roll motion displacement and η_{4a} stands for its amplitude.

However, if we consider sloshing moment in a scope of ship rather than only inside the tank and include the effect of ship natural frequency and its oscillation, then when ω_t is not very close to unity, things can be different to some extent as presented in figure 5[11]. When the ship is excited and resonated at a frequency different from the natural frequency of fluid, it means the excitation amplitude is maximized while the phase lag is not near $\pi/2$. This is dangerous for ships, since the sloshing water motion with phase lag in this range can contribute to a heeling moment, and its amplitude will is proportional to the amplitude of the ship motion which is resonating with the external excitation force. In this situation, the heeling effect caused by phase lag is amplified by the resonance between ship motion and external excitation. Consequently in figure 5, high values of RAO can be observed in cases of $\omega_t = 1.28$ and 0.88 when tuning factor is different from 1. And in these cases, heeling moment is significant lowering the ship stability. Additionally, when the excitation frequency is very slow, namely in quasi-static condition, the tank motion is considered extremely slow which can be seen as static, and the water plan can be regarded as horizontal. In this theoretical condition, the sloshing moment is always in the same phase as tank motion is and has the same sign. In the perspective of energy, there is only energy transmission between the tank and fluid but no loss since no sloshing exists. In other words, there is no water-tank interaction, and energy does not dissipate into heat. In this way, the quasi-static water moment does not have a damping effect on the tank motion in general.

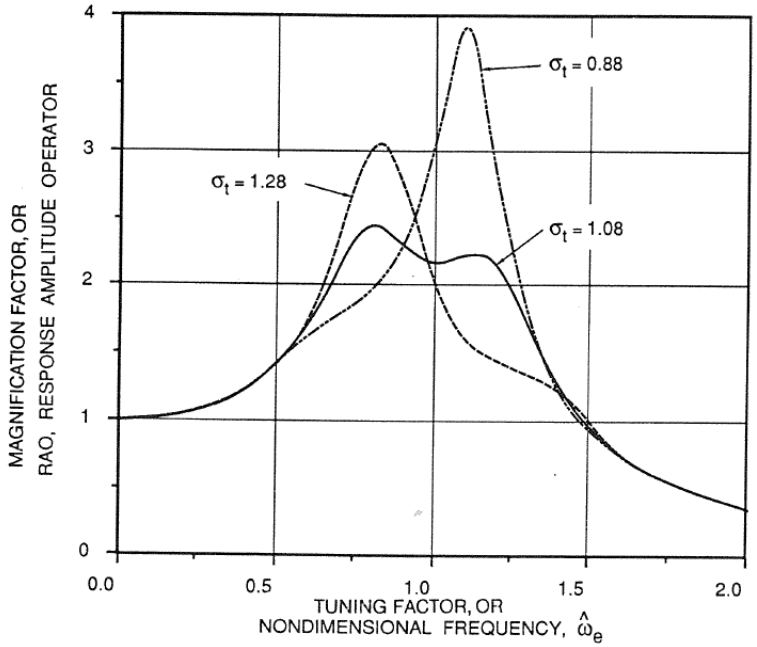

Figure 5: Effect of stabilizer, namely the tank, on the ship stability[11].

Exceptionally, in transient condition, the lag between the tank motion and fluid motion is uncertain and hard to predict since both of their motions change non-linearly all the time. That either the fluid damps the water depends on how the lag evolves throughout the transient tank motion. There is also the possibility that the flooding water increases the roll motion.

2.2 Simplification for the simulation

The original case in the work[14] is a damaged ship with flooding water in the compartment due to the collision with other ship. The impact causes the damaged ship a heeling angular momentum so that it has a roll angle at the beginning. There is also interaction between the ship motion and ocean water. And as the water floods into the compartment of the ship, it flushes on the hull with certain momentum, which can be seen as the inflow effect. In addition, the flooded-in water couples with the compartment motion and exert an moment on the hull as well. Since the depth of flooding water rises, the frequency of sloshing water will change, and the exerting moment will change accordingly[4]. To consider and fulfil all these interaction and effects in both of the tank experiment and simulation[14] is too complicated and difficult. Some simplification is implemented on the tank tests[14].

In the work[14], firstly the inflow effect is neglected. In the experiment and simulation, the compartment is considered intact. The damage on the ship will be added in and studied in other work[13]. As for the interaction between the ship and external water, it is included in the experiment. Finally, the tank experiment[14] is consisted of a series of tank tests using intact compartment freely decaying in calm water with different water amounts and a heeling angle at the beginning. The

heeling angle is triggered by collision or grounding. The tank decaying motion of my case is recorded and will be applied in my simulation. Since the damage on the ship is not of interest, only the resulting heeling angle is taken into account in the test. In this thesis, what of interest is the flooding water motion that interacts with the free decaying tank motion, and the tank is the only object that the flooding water interacts with. Therefore, the only thing that matters is that the fluid interacts with the same tank motion as in the tank test. Straightly applying the recorded tank motion saves lots of time and avoids potential problems while the simulation outcome is uninfluenced. Additionally, this simulation will be conducted in 2-dimension condition. The reason is that 3-dimension simulation considers far more details and require exponentially more computation resources, which is this work cannot afford.

2.3 Computational Fluid Dynamics in general

Typically, CFD methods solve hydrodynamic problems basing on governing equations and boundary conditions. According to the initial boundary condition and governing equations, solution of next time step comes out such as velocity, pressure, boundary condition, etc. Then by applying the new solution into the governing equations, solution can be renewed for further time step. Iterating step by step, the complete hydrodynamic evolving process could be eventually predicted.

The methods can be generally divided into two classes according to the applied governing equations. One uses mass conservation equation and potential theory as governing equations, e.g. BEM(Boundary Element Method). Velocity potential and Laplace equation have to be satisfied while applying this type of methods. The other utilizes mass conservation equation and NS(Navier-Stokes) equations which may be applied in forms of Lagrangian or Eulerian and often with some approximation. This type of methods can be further divided into 2 branches with respect of grid. First one is called *Particle method*, e.g SPH(Smoothed Particle Hydrodynamics) [12], which is a gridless method and traces all the individual particles that represent water. The work load depends on how many particles it traces. The second one is *Grid method* where mesh is built, and the variables like velocity and pressure of cells are calculated. Examples are FDM(Finite Difference Method) and FVM(Finite Volume Method). Similar with *Particle method*, *Grid method* bases its computational load on the density of the grid and the number of cells[4].

For FVM, which is the CFD method I will use, it requires free surface boundary condition to be constantly renewed for the iterative calculation. The method I will apply for surface tracking is known as *front-capturing method*. It does not directly follow the free-surface but takes advantage of some other information to locate the interface. It comprises many sub-methods including VOF(Volume of Fluid), LS(Level Set) and so on. The most obvious benefit of *front-capturing method* is its computation-saving feature. But it also has disadvantage that is numerical diffusion. Numerical diffusion is caused during the mathematical interpolation operation, which leads to the smearing of the interface. It can bring trouble on computational accuracy and even errors in the simulation. According to previous study and experience, refining the grid is well-recognized and effective way to help decrease diffusion[4][9].

This study is aiming at the research of the shallow water sloshing using interDyMFoam which is one of the many solvers of OpenFOAM. It utilizes FVM and VOF to solve and capture the free-surface[9].

3 Research material and method details

In this section, theory about the specific methods that are going to be applied for my simulation will be presented.

3.1 Finite Volume Method

In Finite Volume Method, the computational domain is discretized into a finite number of contiguous control volumes(CVs). At the centroid of each of the CVs, the variable values are calculated. Interpolation is used to find the variable values at the surfaces of the CVs, and approximation is applied to attain the surface and volume integrals. Two sets of governing equations, which are mass conservation equation and Navier-Stokes(NS) equations for incompressible fluid, are applied as tools to calculate the variable values. Since it is simulated under a 2-dimension condition, the mass conservation equation for incompressible fluid is[4]

$$\frac{\partial u}{\partial x} + \frac{\partial v}{\partial y} = 0 \tag{3}$$

and NS equations for incompressible fluid[4] are:

$$\begin{aligned} \frac{\partial u}{\partial t} + u\frac{\partial u}{\partial x} + v\frac{\partial u}{\partial y} &= -\frac{1}{\rho}\frac{\partial p}{\partial x} + \nu(\frac{\partial^2 u}{\partial x^2} + \frac{\partial^2 u}{\partial y^2}) \\ \frac{\partial v}{\partial t} + u\frac{\partial v}{\partial x} + v\frac{\partial v}{\partial y} &= -\frac{1}{\rho}\frac{\partial p}{\partial y} + \nu(\frac{\partial^2 v}{\partial x^2} + \frac{\partial^2 v}{\partial y^2}) \end{aligned} \tag{4}$$

Where u and v indicate the local velocities in x and y direction, and p denotes the local pressure. ρ is the fluid density.

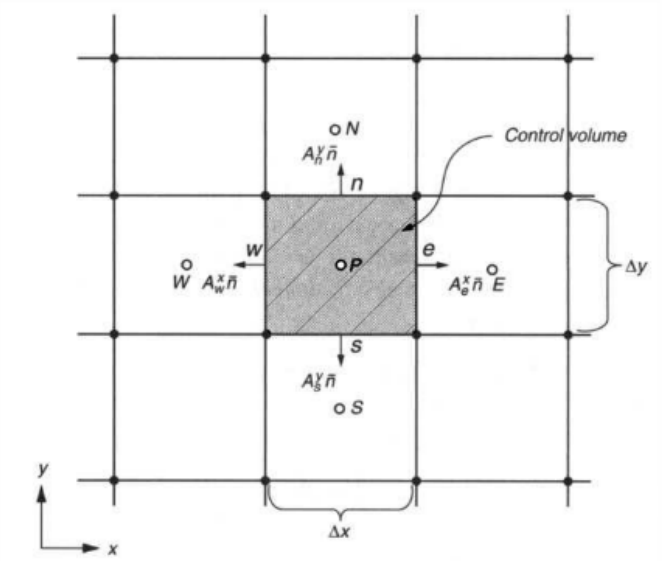

Figure 6: configuration of control volumes[18]

In the figure 6, the CV of interest is marked as P, and the nearby CVs are respectively marked as W, E, N and S. ϕ indicates all the variables of interest like velocity and pressure. The area of the walls of P is A, and the normals to the walls are $\bar{n}$. By interpolation, the variables on the centers of CV walls can be expressed as ϕ_P^W, ϕ_P^E, ϕ_P^N and ϕ_P^S. $\triangle V$ is defined as the volume of CV.

The properties or variables, namely ϕ, of the fluid are calculated at the centroid of the CVs, and then the variables on the walls of the CVs can be solved by interpolation combined with the variables at the neighbouring control volume centroids. Since there are terms consisted of first- and second-order derivatives with respect to time and local spatial location x, y and z in NS equations, it is difficult to solve these derivatives. By applying Gauss' divergence theorem on the CVs, we can derive the derivatives of the variables at CVs' centroids by applying the variables on the control volume walls. Gauss's divergence theorem that applied on the CVs can be written as [18]:

$$\frac{\partial \phi}{\partial x} = \frac{1}{\triangle V} \int_{\triangle V} \frac{\partial \phi}{\partial x} \, dV \; = \frac{1}{\triangle V} \int_{A} \phi \, dA^x \; \approx \frac{1}{\triangle V} \sum_{i=1}^{n} \phi_i A_i^x \tag{5}$$

In this equation, i denotes the surfaces of the CV and n stands for the number of surfaces of the CV. Superscript of A indicate that in which direction the surface area projects. By using an approximation that $\frac{1}{\triangle V} \int_{A} \phi \, dA^x \; \approx \frac{1}{\triangle V} \sum_{i=1}^{n} \phi_i A_i^x$, the derivatives are found by using the variable at the centroids of the CVs of interest and neighbouring CVs.

To numerically solve the governing equations by Time-Marching Method, derivatives of variables with respect to time are needed. However, since the fluid is treated as incompressible flow, the original time derivative of density has been removed in mass equation, which is the key to link the change of pressure through state equation. Consequently, it is not possible to solve the pressure field by time-dependent methods without adaptation due to the lack of time derivative of pressure in governing equations. Thus, the pressure correction method is applied, which is an iterative process. At the beginning, a guessed pressure field p_i is generated. Then according to momentum equations 4, solution of velocities, u and v, should be found correspondingly. As the velocity solution is a result of guessed pressure field, it probably does not obey the continuity equation, so the velocity field will be inserted into continuity equation for correction for mass balance. Accordingly, the guessed pressure field will be corrected based on the necessary correction on the provisional velocity field. However, this cannot be done by simply applying momentum equations because it is too complicated as a linking equation between pressure and velocity. In pressure correction, NS equations will be approximated or simplified so that we are able to modify the pressure field. Afterwards, a new solution of pressure field p_{i+1} is obtained by solving the discretized and approximated momentum equations, and this enables next round of iterative calculation to proceed. Finally, the iteration will end when the velocity field calculated from the guessed pressure field can respect the mass equation within a very limited tolerance[5][8].

Moreover, to solve those variables in equations with respect to time, Euler time scheme is applied in my case, which is an implicit first order time scheme. And

backward time scheme is also applied during the simulation, which is an implicit second order time scheme.

Euler's method is the simplest of the finite difference methods for solving differential equations. Assume y is some variable of interest and we consider the equation

$$\frac{dy}{dx} = f(x, y).$$

Suppose we know y at some starting value of x, then we can find the tangent to the solution at this point by evaluating $f(x, y)$. We now move in the direction of the tangent by a small amount. If the change in x is Δx, then the change in y along the tangent direction is given by

$$\Delta y = f(x, y)\Delta x$$

It gives us a new point on an approximate solution to the differential equation. This process is repeated until a desired value is reached[10].

Clearly the numerical solution depends on Δx. And in general, it is expected that the smaller Δx is, the closer the numerical solution is to the exact solution. But the cost is increased computational time. The method mentioned so far is called Euler forward implicit method. In practice it is usual that y is unknown except for the initial start point y_0 at x_0. Using the iterative process:

$$x_{n+1} = x_n + \Delta x$$

$$y_{n+1} = y_n + f(x_n, y_n)\Delta x,$$

it can finally find the solution of interest even the function of y is never explicitly solved.

In OpenFOAM, Euler time scheme stands for Euler backward time scheme which based on the equation

$$y_{n+1} = y_n + f(x_n, y_{n+1})\Delta x.$$

This is slightly different as it solves the equation involving current state and later one. It is comparably more accurate but more time-consuming at the same time. Both forward and backward Euler methods are called the *implicit Euler method* since the expression of y is not explicitly found[6].

3.2 Volume of Fluid Method

In this research, VOF is applied to capture the free-surface. It calculates a fraction F at each CV, which illustrates the ratio between the fluid volume and total volume of the CV. The fraction varies from 0 to 1. If the CV is full of fluid, then F equals to 1, or F equals to 0 if it is empty of fluid. when the free-surface, or the interface, is within the CV, the fraction is a value between 0 to 1[9].

VOF calculates the values of F in each CV while the mass conservation equation is satisfied, which makes *front-capturing method* reliable and convincing. CVs with F other than one and zero must be where the interface locates, and to depict the shapeof the free surface, the normal direction of interface is needed. The normal

direction is also the direction in which function F changes most rapidly, the gradient direction. When both the normal direction and the value of F are available, a line that is in the same direction of the interface and cutting the CV according to the value of F can be constructed to demonstrate the shape of interface within this CV[9].

Nonetheless, we still need algorithm to compute the evolution of the field function of F. The corresponding equation in 2-D condition is

$$\frac{\partial F}{\partial t} + u\frac{\partial F}{\partial x} + v\frac{\partial F}{\partial y} = 0 \tag{6}$$

As the velocity solution is provided by FVM, this equation of function F is available. Due to possible numerical diffusion, the interface between air and water could become very thick and blur, which may affect the simulation accuracy substantially. Thereby in OpenFOAM, the algorithm is developed by adding an extra artificial term $\nabla F(1-F)\vec{v}_{r\alpha}$ into equation 6 so that we have[9]

$$\frac{\partial F}{\partial t} + \nabla \cdot (F\vec{v}) + \nabla F(1-F)\vec{v}_{r\alpha} = 0 \tag{7}$$

The added term is aiming to compress the interface to diminish the effect of numerical diffusion. This artificial term contributes only when it is close to the interface where F is not zero or one, making $F(1-F) \neq 0$ and it does not affect region outside interface zone. $\vec{v_{r\alpha}} = \vec{v_w} - \vec{v_a}$ indicates the relative velocity at the interface between the two phases, air and water. [1][17] In OpenFOAM, this artificial term is controlled by a factor called cAlpha, and it is proportional to cAlpha in the simulation calculation in the CFD calculation. When cAlpha is 1, it is defined that the interface is normally compressed, and any value of cAlpha larger than 1 means it is overcompressed while values below 1 indicate it is undercompressed. cAlpha takes zero means the artificial term vanishes, and the interface is not compressed by any extra added term. Numerical diffusion could be a problem for simulation however in that case.

The numerical diffusion comes from the approximation made for interpolation by FVM while calculating velocity and some other properties. There are some second-, third- and even higher order errors generated which lead to numerical diffusion and dispersion. However, one proved efficient way, as have mentioned, is to refine the grid to minimize the diffusion[9].

3.3 Related fluid mechanics

In this study I am trying to work out a reliable and fast numerical simulation for the shallow water sloshing case. Some fluid mechanics effects may be important for a dependable simulation of the case, even though calculating them may take more computation resources. I will elaborate them in the following part so that it may help to understand the effects and make the tradeoff in simulation for optimization.

3.3.1 Viscosity

The viscosity or the friction between the water and solid body is a very important character to consider. In 2D condition, for a flow past a fixed body with velocity

U_∞, let us take local coordinate so that x and u are the position and velocity along the body surface respectively, and y and v are the position and velocity normal to the body respectively(y=0 on the body). Potential-flow theory assumes a solid body in the fluid is impermeable and a tangential velocity exists along the body, namely $u = U_e$. This is called free-slip condition since it ignores the viscosity. In reality, the fluid velocity at the body surface has to be equal to the body velocity, namely zero, which is shown in figure 7. This is called no-slip condition. Under this condition, u goes from U_e to zero within a certain distance from the body. This layer of fluid is called boundary layer[22].

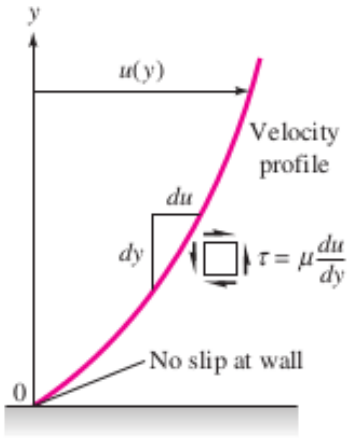

Figure 7: boundary layer [22]

Inside the boundary layer, there is the shear/tangential stresses which is in the form of

$$\tau = \frac{\mu \partial u}{\partial y}.$$

This shear force is proportional to the slope of the velocity profile in figure 7 and reaches its max value at the body surface[22]. For a blunt body, due to the flow separation, the pressure difference at the front and rear ends can be significant, and the pressure drag force may dominant. To slim body like my case which has a flat plane at the bottom of the tank, the viscous drag force matters.

3.3.2 Surface tension

Surface tension plays a significant role on the interface problem. It makes the free surface of the water act like a stretched elastic membrane.

Theoretically, surface tension comes from the cohesive force between liquid molecules. The cohesive forces are shared with all neighbouring molecules, and the molecules also repel each other due to the close packing. Water molecules are relatively loose at the interface and they attract each other there. Since half of their neighbours are missing at the interface, the forces from other water molecules appears to be tension[22]. Due to the surface tension, when an object is on the surface of the

fluid, the surface under tension will behave like an elastic membrane. Consequently it gets harder to penetrate it.

To describe the surface tension, concept is made: "if a cut of length dL is made in an interfacial surface, equal and opposite forces of magnitude $\Upsilon\ dL$ are exposed normal to the cut and parallel to the surface, where Υ is called the *coefficient of surface tension*."[22] Its value is related with temperature, and at 20 °C it is measured as 0.073 N/m for air-water interface. Then I would like to introduce a dimensionless parameter called Weber number(We). This number is important only if it is equal to one or less, which typically occurs when the surface curvature is comparable in size to the liquid depth. It decides that if the surface tension matters, too. According to its expression

$$We = \frac{\rho U^2 L}{\Upsilon},$$

where L is the characteristic length and U is the fluid velocity. I am able to consider if the surface tension matters. In the my simulation, the size of bubbles varies from 1 mm to 7 mm. For those bubbles smaller than 4 mm, some of them move at the speed below 0.1 m/s. For instance, they can be observed in figure 8 and 9. Each cell in the figures is around 1 mm wide and 1 mm high. The time for the figures is 1 second after the first impact, and the corresponding We is equal to around 0.55 which is smaller than 1. Consequently, it is necessary to consider the surface tension and check its influence in the simulation[22].

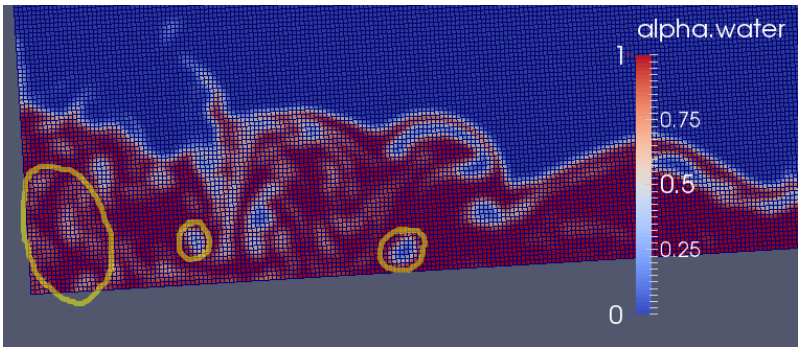

Figure 8: Fluid behaviour

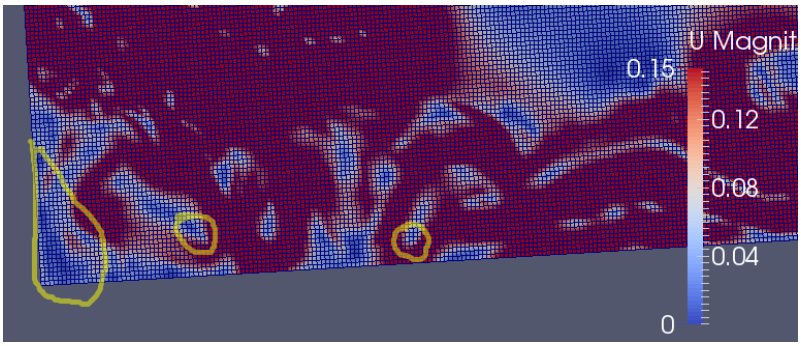

Figure 9: Velocity magnitude contour

3.4 Reynolds-Averaged Navier Stokes

The state of fluid motion can be classified as laminar flow and turbulent flow. In laminar regime, fluid moves in order and the flow is smooth, whereas in turbulence regime, the flow behaviour becomes randomly fluctuating and agitated. All the flow properties such as velocity fluctuate disorderly, ranging from 1 to 20 percent of the average value when it is fully turbulent. According to the description for flow regimes, the flow regimes are decided by Reynolds Number(Re) mainly, which is defined as $Re = \frac{VL}{\nu}$. V is the fluid velocity, ν is Kinematic Viscosity. In my case it is the width of the tank. When Re is between 10^3 to 10^4, the fluid is in the transition from laminar to turbulence, and it acts as turbulence when Re goes beyond 10^4[22].

In turbulent case, we can still apply Navier-Stokes equations and solve them numerically. But, it is too complicate to do so. In turbulence, there are a lot more details to solve with NS equations, and it requires more computation resources. Actually, it is also not necessary to solve all the turbulence details. CFD users are almost always satisfied with the time averaged solution of fluid properties like velocity and pressure[20].

In Reynolds-Averaged Navier-Stokes equations, velocity, pressure and some other properties are decomposed into two parts, $\varphi(t) = \Phi + \varphi'(t)$. It is assumed that there are a mean term that is time averaged constant:

$$\Phi = \frac{1}{\triangle\, t} \int_0^{\triangle t} \varphi(t)\, dt \tag{8}$$

and a fluctuation term with a time averaged value of zero

$$\bar{\varphi'} = \frac{1}{\triangle\, t} \int_0^{\triangle t} \varphi'(t)\, dt \equiv 0. \tag{9}$$

Insert the above expression for velocity and pressure into time averaged Navier-Stokes equation over a time period. The period should be larger than the time scale associated with the slowest variations of property φ. Here comes some additional terms called Reynolds stress terms from the time-averaging convective acceleration term in momentum equations. To use $\varphi(t) = \Phi + \varphi'(t)$ to express velocity, then it writes $\mathbf{u} = \mathbf{U} + \mathbf{u'}$for the total velocity. The time-average momentum equation in x direction can be written as

$$\frac{\partial U}{\partial t} + div(U\mathbf{U}) + div(\overline{u'\mathbf{u'}}) = -\frac{1}{\rho}\frac{\partial p}{\partial x} + \nu \cdot div(grad(U)) \tag{10}$$

and the rest equation for y direction is similar[20][15].

Reynolds stress terms is the third term in equation 10. It makes it almost impossible to solve the equations since the unknowns greatly increased while the number of equation stays the same. In order to work out RANS equations, presumption is made that Reynolds stress terms can be treated as an analogy of conventional viscous stresses so that only one more unknown appears in the equations, the eddy viscosity μ_t[15][20].

In my case, it is expected that most of the fluid motion is in turbulence flow regime. However, establishing and running a turbulence case requires a more powerful computer. The only choice is to simulate the fluid in laminar.

3.5 Model & grid establishment

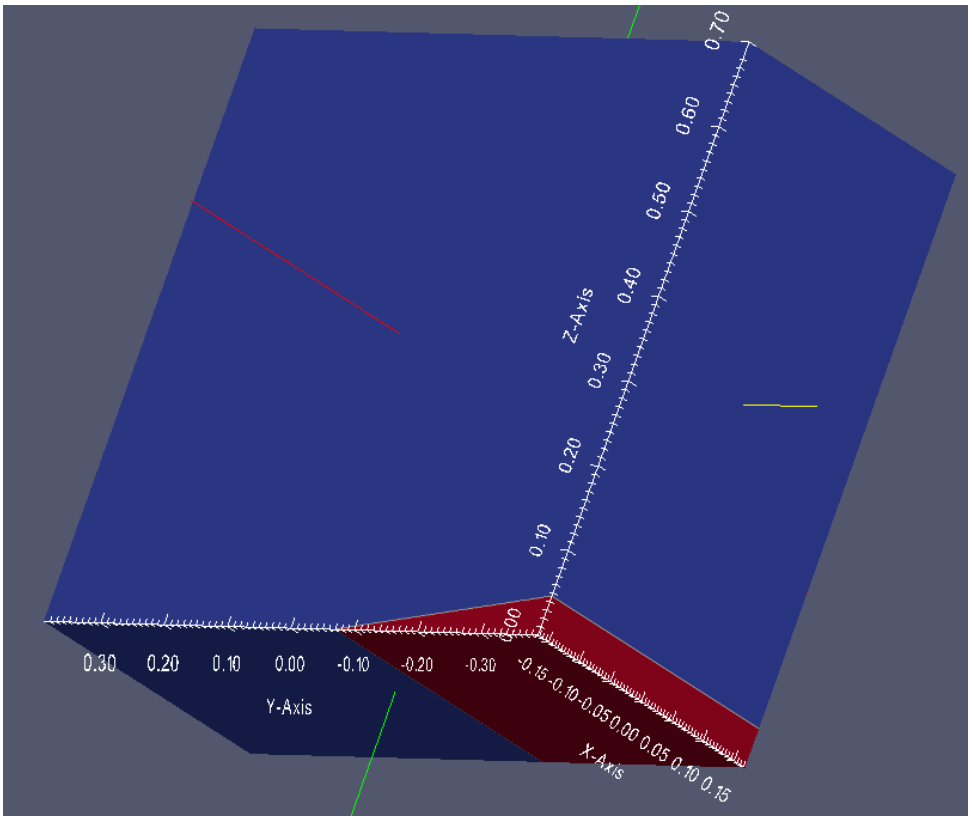

Figure 10: Dimension of the tank

The simulation model is based on the tank sloshing test that Lumped Mass method failed to predict. The size of the tank is 700 mm×780 mm×335 mm, which stands for *depth* × *breadth* × *longitudinal length* of the tank. The tank test is conducted with 2.5 kg water inside, which indicates a filling ratio(h/B) of 0.012. The tank is forced to roll in transient motion, starting with an inclined roll angle of 8.151 degrees and from right side rolling to the left side. The tank model is presented in figure 10 with the real dimension. Since I simulate the sloshing water in the tank under 2D condition, the water motion in X-direction shown in figure 10 is neglected so that there is only one cell covering that dimension in the model.

In figure 10 the red volume represents the water while the blue is air. By the simulation afterwards, it proves that throughout the sloshing, water never reaches anywhere higher than 70 mm from the the bottom. Thus, in order to save the computational capacity, I halve the tank depth. Moreover, I divide the computation domain into four sub-domains vertically with different mesh size as can be seen in figure 11. In figure 11, the orange lines highlight the interfaces of the sub-domains. The figures in yellow on the left side are the grid densities in the form of *horizontal cell number* × *vertical cell number*, while the numbers at the bottom and on the right are dimensions of the sub-domains. Between each computational sub-domain, the mesh size difference cannot be very large. In this sense, the lowest

grid domain is 70 mm high meshed by 800×70 ($horizontalcells \times verticalcells$). And the upper domain is 20 mm high with cell density of 400×10. Then there follows another domain with also 20 mm height and 100×3 grid density, while the top domain ends at the mid of the tank height, namely with 240 mm height and a grid of 40×15.

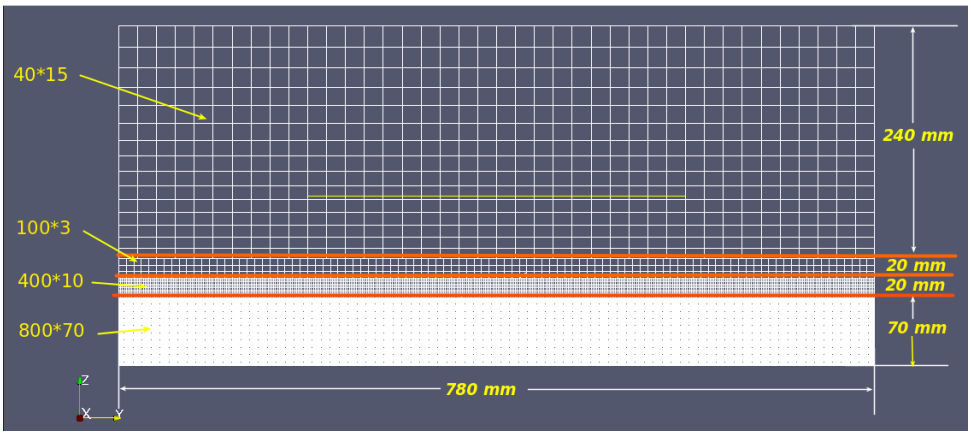

Figure 11: Grid setup

The reason drives me to implement such setup is that the air motion actually barely influences the fluid motion. It is a waste to calculate such a comparatively large space full of air. Furthermore, even after I have halved the tank depth, it is not necessary to mesh the remaining vast air space with a dense grid. The vertical division of computational domain can more effectively take advantage of computation capacity. A series of simulation has been done proving that this setup does not influence the fluid motion and moment prediction.

3.6 Simulation methods

Table 1: Setup of all the simulations

Identity	Grid	cAlpha	BC	surface tension	ddt scheme	Time step
S1	800×70	0.8	no slip	none	Euler	0.004s
S2	320×32	0.8	no slip	none	Euler	0.004s
S3	400×40	0.8	no slip	none	Euler	0.004s
S4	1000×70	0.8	no slip	none	Euler	0.004s
S5	1200×70	0.8	no slip	none	Euler	0.004s
S6	1400×140	0.8	no slip	none	Euler	0.004s
S7	800×70	0.8	no slip	applied	Euler	0.004s
S8	800×70	0.8	no slip	applied	backward	0.004s
S9	800×70	0.8	free slip	applied	Euler	0.004s
S10	800×70	1.0	no slip	applied	Euler	0.004s
S11	800×70	1.2	no slip	applied	Euler	0.004s
S12	800×70	1.5	no slip	applied	Euler	0.004s
S13	800×70	0.8	no slip	applied	Euler	0.001s
S14	800×70	1.0	no slip	applied	Euler	0.001s
S15	800×70	1.2	no slip	applied	Euler	0.001s
S16	800×70	1.5	no slip	applied	Euler	0.001s
S17	800×70	0.8	no slip	applied	Euler	0.002s
S18	800×70	1.0	no slip	applied	Euler	0.002s

Based on the grid setup, a series of simulation is conducted as presented in table 1. Since the bottom grid domain is of the most significance, here in the table only the bottom grid density is specified, and BC in the table stands for Boundary condition in short. As mentioned previously about equation 7, There is an artificial term used to compress the interface to diminish the diffusion. In OpenFOAM, there is a coefficient named as cAlpha that is used to control that artificial term. Attention should be paid that cAlpha is chosen as 0.8 as a start point in these simulations since there are some obvious ripples on the free surface in case S1 once cAlpha is larger than 0.8. Unsuitable cAlpha may overcompress the small waves or deformation at the free surface and lead to unphysical ripples such as shown in figure 12.

If mesh is refined, the simulation quality will increase in general. However, after the quality of the mesh reach certain level, this kind of improvement will become very limited, and further refining of the grid can hardly effectively improve numerical calculation. This is called convergence. Simulations from S1 to S6 are the convergence

test, aiming to find the grid threshold that has the least cells and provides good result. In my case, the simulation result of interest is the sloshing moment history. Considering the possibility that simulation result may have already converged at a coarser grid, S2 and S3 are conducted to verify how the results will be by applying coarser grids than S1.

Figure 12: Appearance of ripples

As mentioned, quasi-static method considers the roll motion as extremely slow. It is often taken as reference when studying the damping effect of sloshing. The forced roll motion of the tank is given in figure 13. Based on the forced motion, quasi-static moment can be attained, which is a function of roll angle. Its history is presented in figure 13.

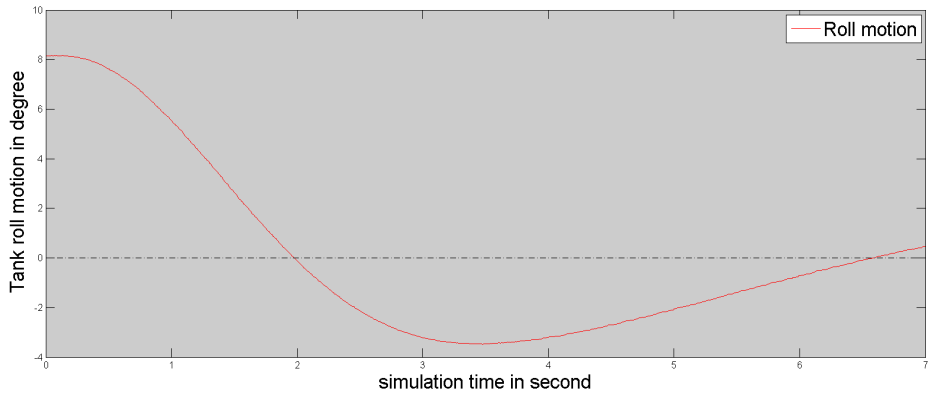

Figure 13: Roll motion of the tank

The shape of the fluid in the tank changes. When the bottom is not fully wet, its shape is wedge, which can be mathematically summarized as the condition that: $V_0 \leqslant \frac{1}{2}|\tan\theta|B^2 \cdot D$ where V_0 represents the volume of water. Mark the rolling angle as θ, D as the tank length in x direction in figure 10, B as the breadth of the tank and b as the length of wet bottom, which are represented in figure 14. Then we always have the relationship as:

$$V_0 = \frac{1}{2}b \cdot |\tan\theta| \cdot b \cdot D$$

. The expression of the arm of the moment can be expressed as

$$Arm_{wedge} = sign(\theta)(\frac{B}{2} - \frac{1}{3}\sqrt{\frac{2V_0}{D \times |\tan\theta|}})\cos\theta$$

Accordingly, with m_{water} as the mass of the flooding water in tank, the moment expression is

$$M_{quasi-static} = sign(\theta)(\frac{B}{2} - \frac{1}{3}\sqrt{\frac{2V_0}{D \times |\tan\theta|}}) \cdot m_{water} \cdot g\cos\theta \tag{11}$$

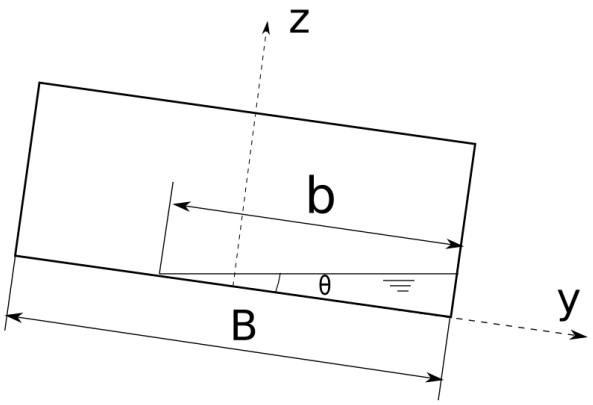

Figure 14: The fluid domain resembles a wedge

And when its bottom is always wet, its shape is a trapezium, which means $V_0 \leqslant \frac{1}{2}|\tan\theta|B^2 \times D$. The expression to calculate the arm is

$$Arm_{trapezium} = \frac{-B^2}{12h^*}\tan\theta$$

where $h*$ is the average height equal to $h^* = \frac{V_0}{B \cdot D}$ as shown in figure 15. The expression for the moment is yielded as

$$M_{quasi-static} = \frac{-B^2}{12h^*}\sin\theta \cdot m_{water} \cdot g \tag{12}$$

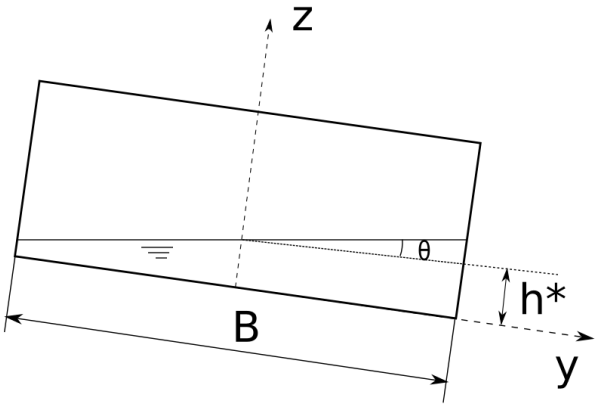

Figure 15: The fluid domain resembles a trapezium

The quasi-static moment completely follows the roll motion in term of sign and phase, which can be observed in figure 16. After the simulation results come out, they will be compared with the quasi-static moment to see how the simulated decaying sloshing moment lags behind quasi-static moment as well as the tank motion. At the same time, to ensure that the simulation result matches reality, the simulated fluid motion will be compared with the tank test images.

Throughout the simulation, different means will be applied aiming to improve the simulation quality. The theoretical thinking behind these improvement will be elaborated in next section with the results. Since there are some 'noises' in the roll motion of tank with high frequency and small amplitude which can be seen in figure 13, it can trigger vibration in the moment prediction, which may decrease the readability. Thus the data are processed and filtered before they are represented. One method is sliding average. It calculates the average value within certain period. It will lead to loss of data in the first and last half period. Another way is low-pass filtering. This removes those data with high frequency. The calculated sloshing moment will be presented in such three forms of original values, sliding averaged values and low-pass filtered values.

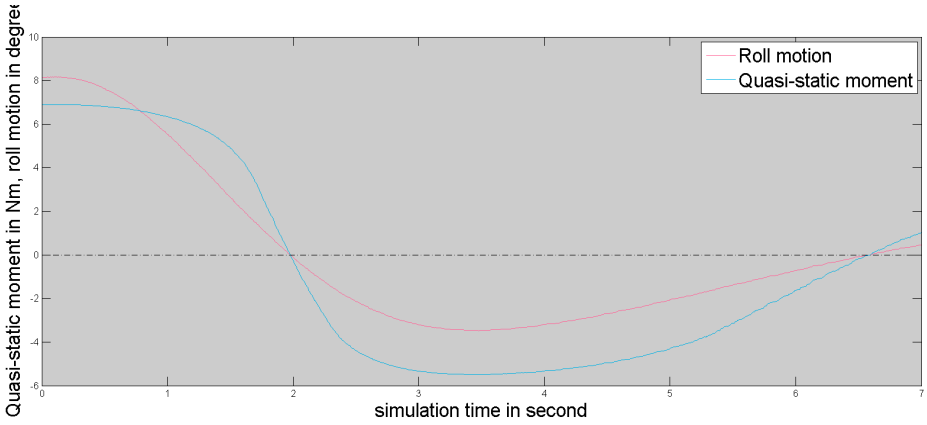

Figure 16: Quasi-static moment

As for simulations, firstly in S7, surface tension is added. And different time schemes are tested to find a potentially more robust and accurate alternative. In S10, free slip boundary condition is tested. Finally, to check possible diffusion and to decrease unphysical phenomena, time step length and cAlpha are changed again.

4 Results

4.1 Convergence test

The convergence test includes simulations from S1 to S6. I extract the sloshing moment history of each case and compare them together in figure 17, 18 and 19. Apart from this, the roll motion and quasi-static moment history are also attached in the figures. According to these figures, it seems the simulation outcome has already converged since there is really not much change made by different mesh density. They basically follow the same trend, all vibrating at the same intensity level and almost overlapping with each other in the figures. Based on the sloshing moment histories for each mesh density, it shows even the loosest grid can provide a good moment prediction as the most refined grid.

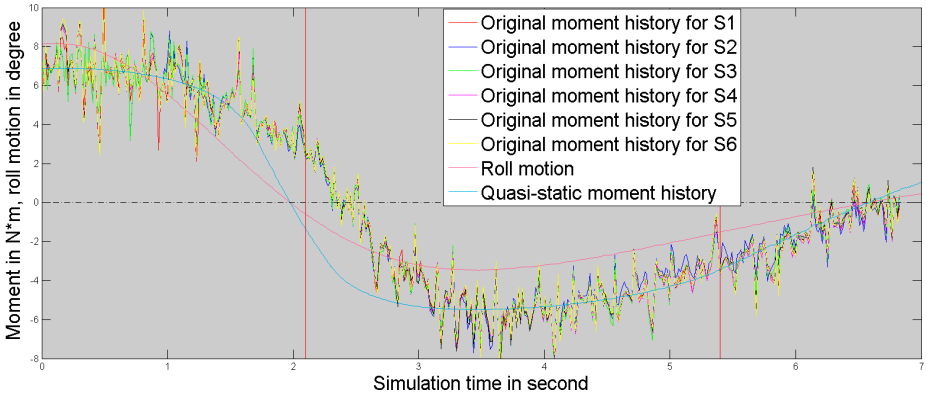

Figure 17: Original moment history for S1-S6

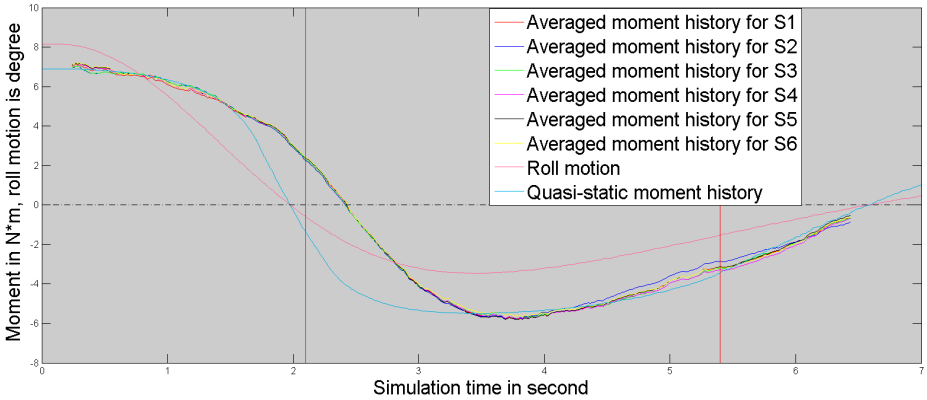

Figure 18: Averaged moment history for S1-S6

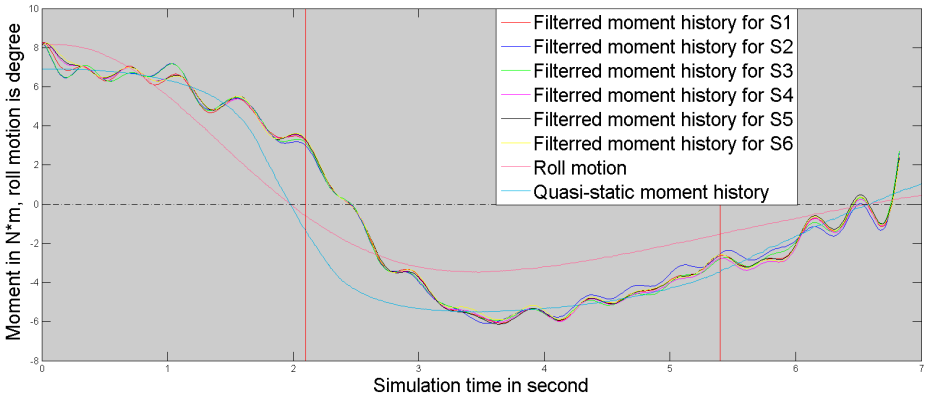

Figure 19: High-frequency-filtered moment history for S1-S6

Then, the image comparison is presented in Appendix A, it seems that higher resolution does not matter much in the simulation in term of the impact time marks. When it comes to coarse mesh, the simulated fluid motion is a bit ahead of the reality right after the impact happens. It can be observed in the image comparison at t = 2.7s. But, generally, this lag is slight and negligible. The general fluid motion of the simulations are almost the same. It matches well with the tank test. The first impacts of all the simulations occur around t = 2.1s and the second one at t = 5.4s, which are very close to the experiment. And the hydraulic jump motion keeps in the same pace as it does in the tank test after t = 3.3 s. However, it is obvious that the interface behaviour and air-water interaction in each case varies quite a lot with respect to the trapped air and water splashing. Moreover, in all the simulations, the free surface behaviour and internal bubble motion are fairly different from the reality. In the tank test, it is hardly observed that there is violent internal water interaction that triggers high water splashing at the interface after the first impact, and far more air is trapped in the fluid, i.e. when t = 3.6 s in figure 21. Some of it unphysically stays inside water for a long period and does not rise to the surface physically.

In S2, due to the coarse mesh, free surface is very blurred and thick. The trapped air bubbles inside the fluid are quite big compared with other cases. However, as mentioned, its sloshing moment histories almost overlaps with others' in figure 18 and 19. The common point among these simulated cases and tank test is the general motion fluid, which means the hydrostatic pressures $p_{hydrostatic} = \rho g h$ and the induced moments are similar. In my opinion, this can be seen as the evidence that the hydrostatic pressure plays a major role in the sloshing moment, while the hydrodynamic pressures generated by impact and other hydrodynamic phenomenon like splashing are of less significance. It is probably because of the limited roll amplitude, and no resonance.

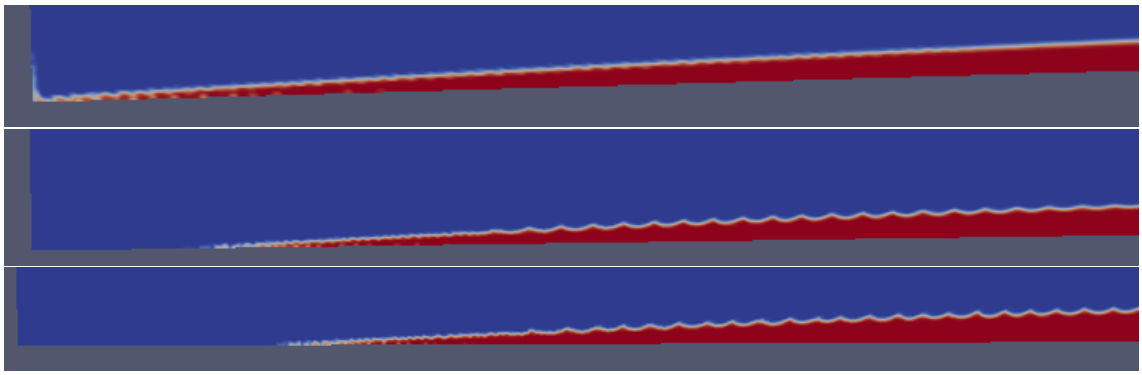

Figure 20: Ripples observed in S1, S4 and S5

Additionally, there are noticeable ripples again in the cases of S4 and S5 at a early stage before water hits the left wall. In consecutive three tests with increasingly refined mesh, S1, S4 and S5, there are more and more obvious ripples observed in figure 20. However, when the cell size of grid is reduced further to S6, namely 1400×140, ripples disappear. One reason might be the inequality of horizontal and vertical cell lengths. When I change the grids of S1, S4 and S5, only the breadth of the cells is decreased while the height keeps the same, which makes the cells not square but rectangular. It is until S6 that I halve the height of cells, and the cells become square again. Correspondingly the ripples disappear. Also, in S1 the cell shape is also very closed to square and its ripples are insignificant.

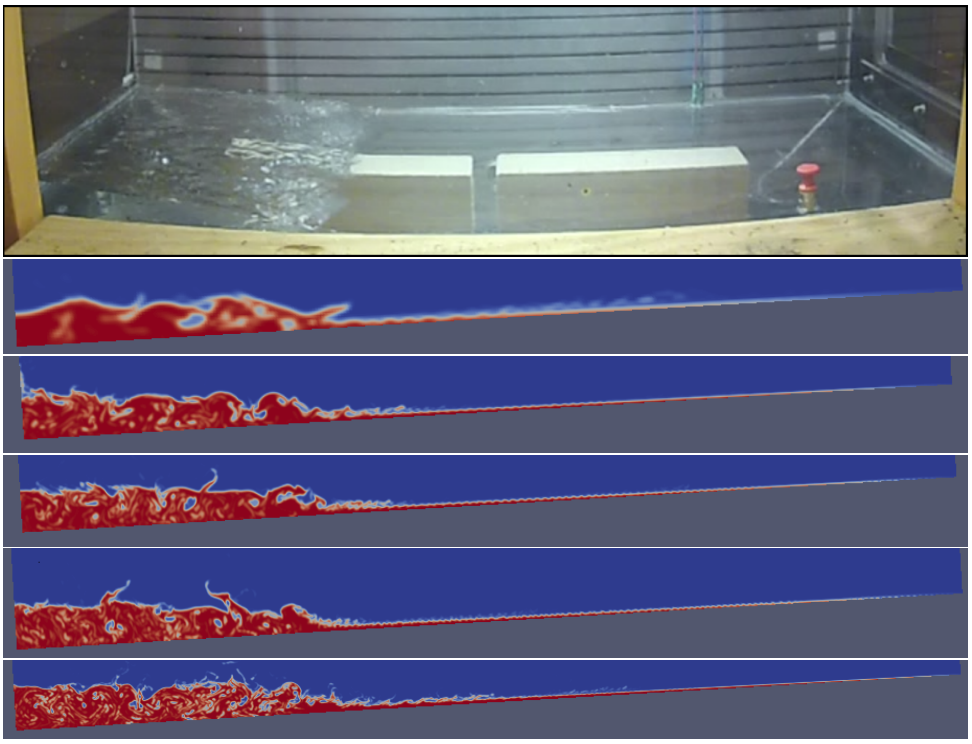

Figure 21: Images for tank test and simulations with S2, S1, S4, S5 and S6 at t=3.6s

Generally, the coarse mesh simulates the water motion details poorly, especially for interface performance, the grid of S1 is selected for the following simulations. It can simulate the sloshing details acceptably well and avoid most of ripples. This is also a result of the tradeoff between simulation quality and computation efficiency.

4.2 Improved simulation

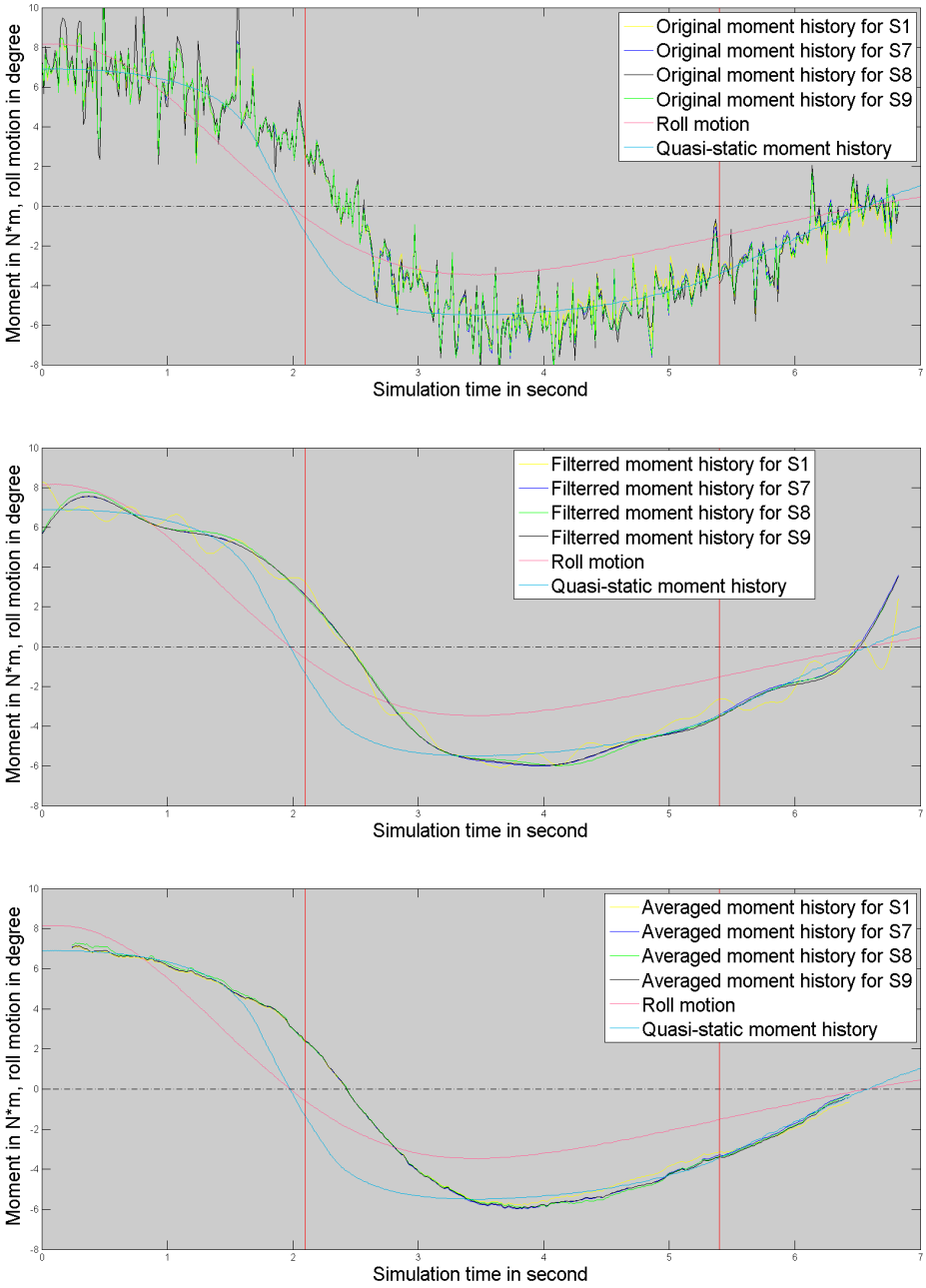

Figure 22: Original, filtered and averaged moment histories for S1, S7, S8 and S9

According to the observation of the simulations so far, air bubbles behaves in an irregular and unphysical way. Those bubbles seem not to be influenced by the buoyancy, instead, they stays near the bottom and can keep barely moving for a period. In S7, surface tension is added to improve this problem.

Surface tension plays a significant role on the interface problem. The idea to add surface tension is aiming to make the surface more compact and robust, which means more viscous effect should be included so that it can prevent excessive air from getting trapped in previous simulation. And actually surface tension works well in this sense.

The sloshing moment histories in figure 22 are presented and compared with the old one. The result shows that there is no any important change. Image comparison is attached in Appendix B. In S7, far less air is trapped inside, and the motion of bubbles is much more physical. Bubbles float and disappear faster and in time. For the interface, the unphysical splashing is also reduced significantly. It is apparent that the surface is more smooth with less water interaction compared with simulations without surface tension, which can be observed in Appendix B when t = 2.85 s to 3.3 s. However, to some extent, excessive entrapped air bubbles and slight unphysical splashing still remain. Furthermore, the hydraulic jump in S7 behaves oddly from t = 3.6 s with a significant solo wave appearing which breaks in an unphysical way a while later. It is still hard to say that the air-water interaction and interface performance have become completely physical in S7.

One thing needs to be mentioned is the fluid motion at the hydraulic jump is very complicated and violently changing. It is presented in figure 23, 24 and 25. When the first impact just happens, the motion is generally clockwise. Afterwards, some part behind the bore starts to move anticlockwise, which in happens at around t = 2.7 s. Finally the fluid motion at the bore becomes totally anticlockwise. This happens after about t = 3.45 s.

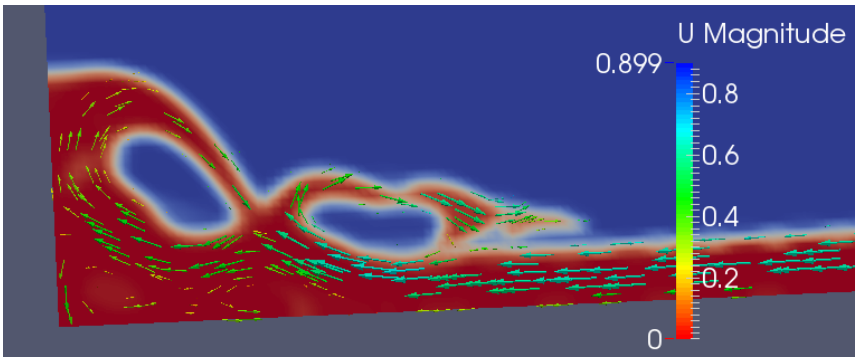

Figure 23: Vector graph for fluid motion velocity in S7 around the bore at t = 2.4 s

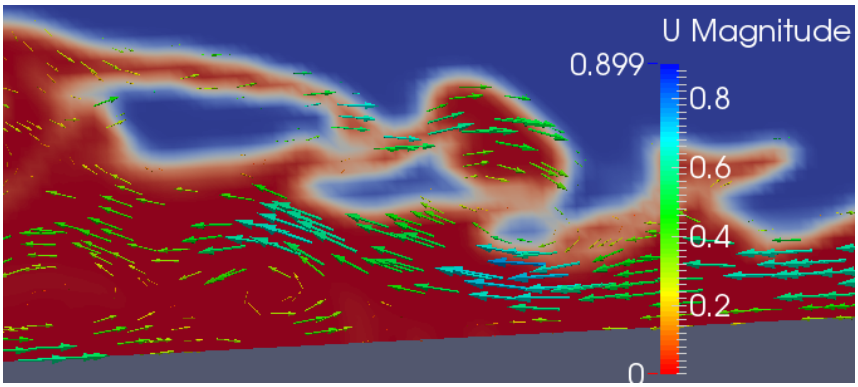

Figure 24: Vector graph for fluid motion velocity in S7 around the bore at t = 2.7 s

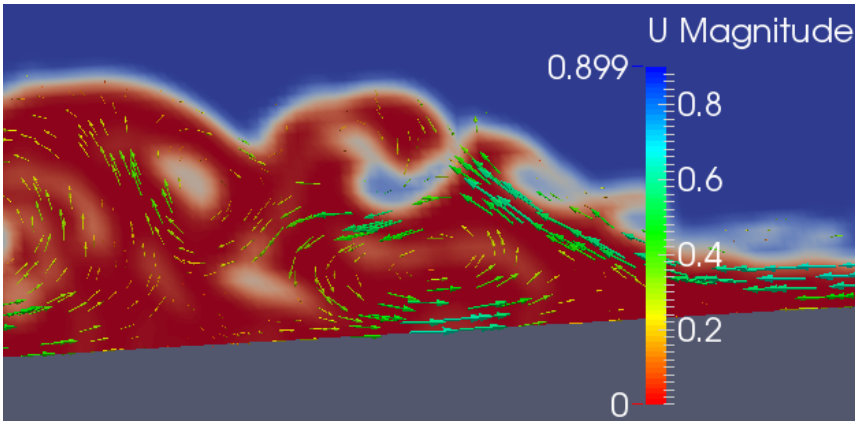

Figure 25: Vector graph for fluid motion velocity in S7 around the bore at t = 3.45 s

So far, there still remains unphysical interface behaviour including limited unreal splashing as well as the abrupt solo wave at the bore. It might be a result of 2D effect. In two-dimension condition, X direction in figure 10 is the dimension that is not taken into account, so all the physical phenomenon in this direction is regarded as uniform in this dimension. An example is figure 26, where the domain is cut somewhere along X direction, and we can see that on the cross section the bubble is uniform along X direction. It means any bubble entrapped in the fluid will push away all the water above before it reaches the free surface and penetrates it. And every time after a bubble penetrates the interface, the water will be pushed away and flow back to recover the empty space. Then splashing happens. This happens in the whole x direction and could make the fluid interaction more wildly than the reality. In three-dimension condition, the air does not act uniformly in x direction. Some bubbles may get together to form a larger bubble while some other may collapse into many smaller ones. The surface does not have to be breached everywhere in x direction due to smaller bubbles, which may contribute to more trivial air-bubble interaction and more smooth interface.

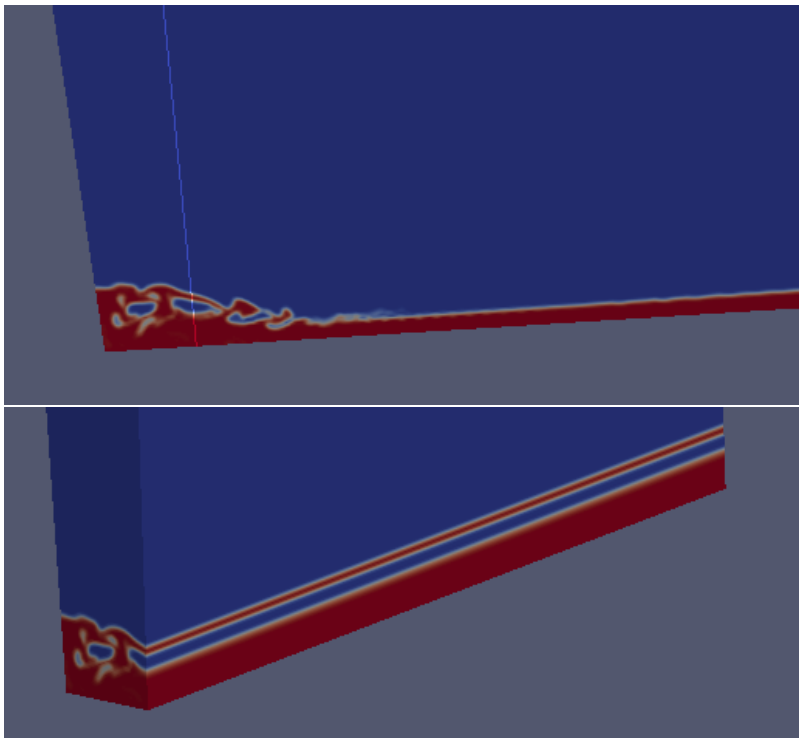

Figure 26: By cutting the tank, the uniform fluid motion in x direction can be seen.

As a result, surface tension improves simulation quality for sloshing water motion prediction, and this makes it always added in the following simulation.

And in S8, according to the recommendation by Jesus Gomez-Goni et al 2013[7], backward scheme is utilized, which is a second-order implicit time scheme. The image comparison is in Appendix B, where we can see there are fairly apparent ripples in the backward case. It can be seen in figure 27. Those ripples actually show up before the impact and lasts till the second impact, existing from t = 1.4s till 7s. Surface tension cannot help improve the ripple problem much in this case. Apart from this, compared with Euler, backward has its advantage. In S8, the unphysical hydraulic jump vanishes, and the behaviour of the hydraulic jump is quite decent as shown in figure 28. Basically, backward scheme does limited improvement, but it brings long lasting ripples at the same time, which is not acceptable.

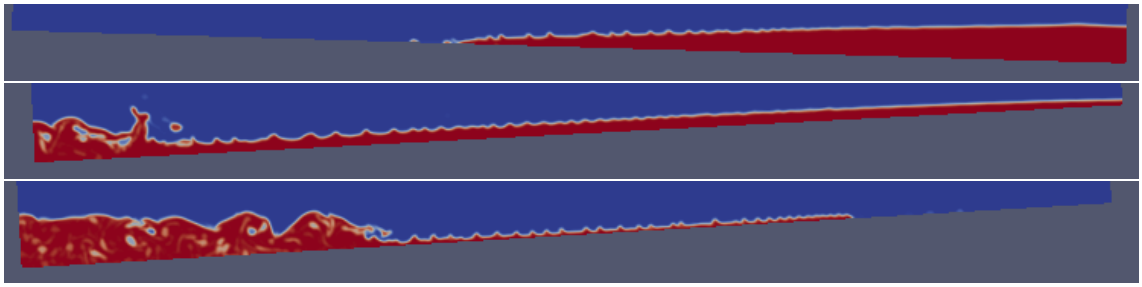

Figure 27: Ripple captured in S8[1] at t = 1.5s, 2.7s and 3.6s

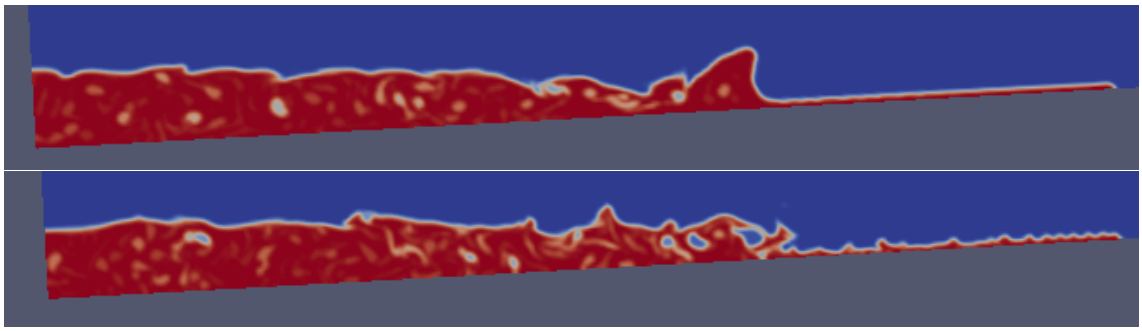

Figure 28: Comparison between S7 and S8[1] at t = 3.9s

The last trial I do is about boundary condition. As in no-slip condition, although the quality of simulation details have been improved quite a lot, problems like excessive entrapped air in the fluid still exist. The hydraulic jump has some unphysical shape and breaks abnormally. The introduction of idea fluid in the potential theory where there is no viscosity on the boundary might potentially help the abnormal behaviour of hydraulic jump and bubbles. However, due to limitation of the capacity of interDyMFoam, which will be specified in the next chapter, I can only set part of the tank boundary as free-slip condition, which is neither a completely practical condition nor theoretical condition. Furthermore, in S9, the result seems to have a very slight improvement. The bubbles move slightly faster than it used to, but the improvement is limited. In the sense of sloshing moment, it can be learned in figure 22 that the moment does not change much. Considering that this partly free slip condition does not coincide with reality and is not theoretically correct, this setting is denied.

4.3 Diffusion check

So far, there are still potential to refine the hydraulic jump behaviour and trapped air. The air is constantly trapped in the water during the impact and afterwards. Here comes an idea that the interface is not compressed enough due to relatively small cAlpha so that the diffusion leads to unphysical free surface behaviour. One way is to check the influence by increasing the cAlpha to verify if diffusion problem troubles. If no improvement shows, then diffusion should not be a key problem here.

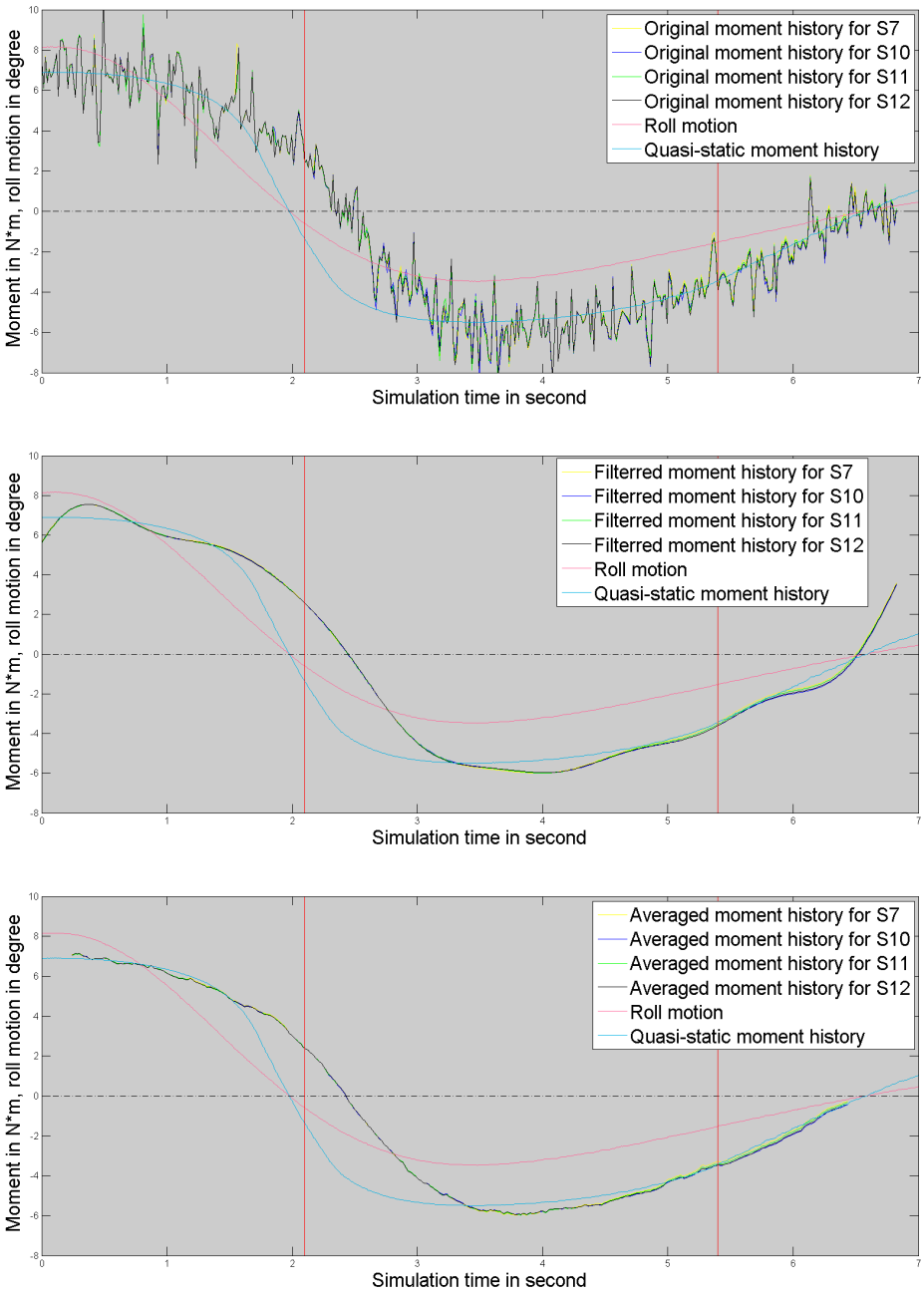

Figure 29: Original, filtered and averaged moment histories for S7, S10, S11 and S12

Currently cAlpha is set as 0.8 to get rid of ripples. In S10, S11 and S12, it will be increased. Corresponding image comparison is attached in Appendix C. From the comparison, fluid motion including the hydraulic jump motion in all the simulations match exactly with the tank test until t = 3.3 s. Afterwards, the unphysical wave shows up again at the hydraulic jump in all the simulations and breaks later strangely. This is illustrated in figure 30 and 31. Besides, the simulated water motion still catch the tank test regarding first impact timing, but it lags behind somehow when the second impact happens.

As expected, in figure 29 the sloshing moment is hardly influenced by different values of cAlpha, all the histories looks identical, which once more demonstrates that fluid moiton details like unphyisical bubbles and the interface performance like odd hydraulic jump shape have a limited effect on the moment.

Generally speaking, increasing cAlpha does not help improve the interface. Since larger cAlpha will lead to harder compression of interface, we can see from the image comparison that at t = 2.25 s ripples show up in S10 as well as S11. The idea to insert larger cAlpha is aiming at diminishing the possible diffusion, but the side-effect is ripples. One possible means to eliminate this is to reduce the time step. It can boost the accuracy of the numerical calculation so that hopefully it can remove the ripples which are a kind of numerical error.

Previously time step is set as 0.004 s, and in S13 to S16, it is decreased to 0.001 s. The simulation result, attached in Appendix D, shows that reducing time step cannot really effectively limit the ripples' appearance. From the result, in the case of S15 there are still obvious ripples at an early stage before the first impact. And S13 and S14 have acceptable ripple phenomenon, which is similar with S7 and S10.

Furthermore, if we put the ripple problem aside, the abnormal big wave observed previously still exists in most of the cases acting in the same manner apart from case S14 with cAlpha of 1.0 under reduced time step condition. In this only exceptional simulation, there is no apparent isolated wave appearing at the hydraulic jump throughout out the simulation as shown in figure 32. It can be regarded as the best simulation so far.

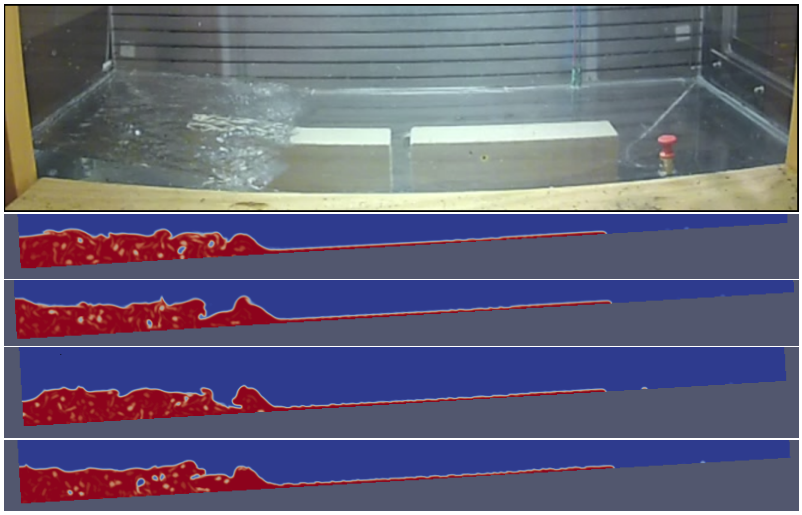

Figure 30: Images for tank test and simulations from S7 and S10 to S12 at t=3.6s

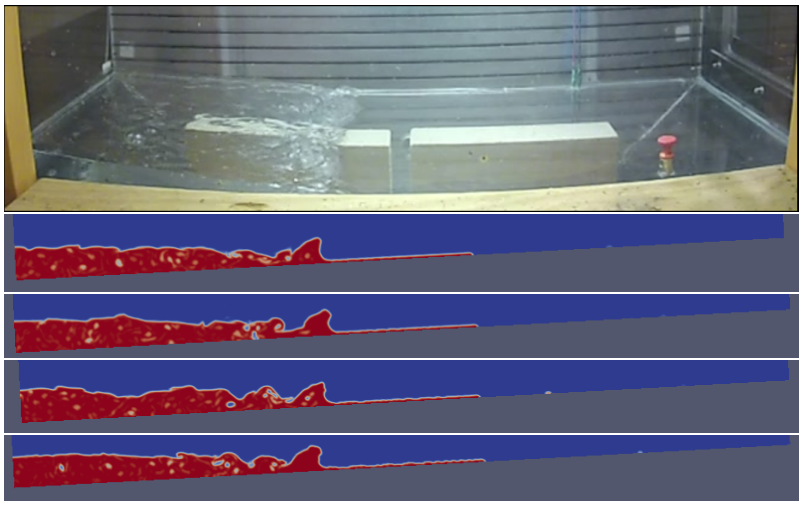

Figure 31: Images for tank test and simulations from S7 and S10 to S12 at t=3.9s

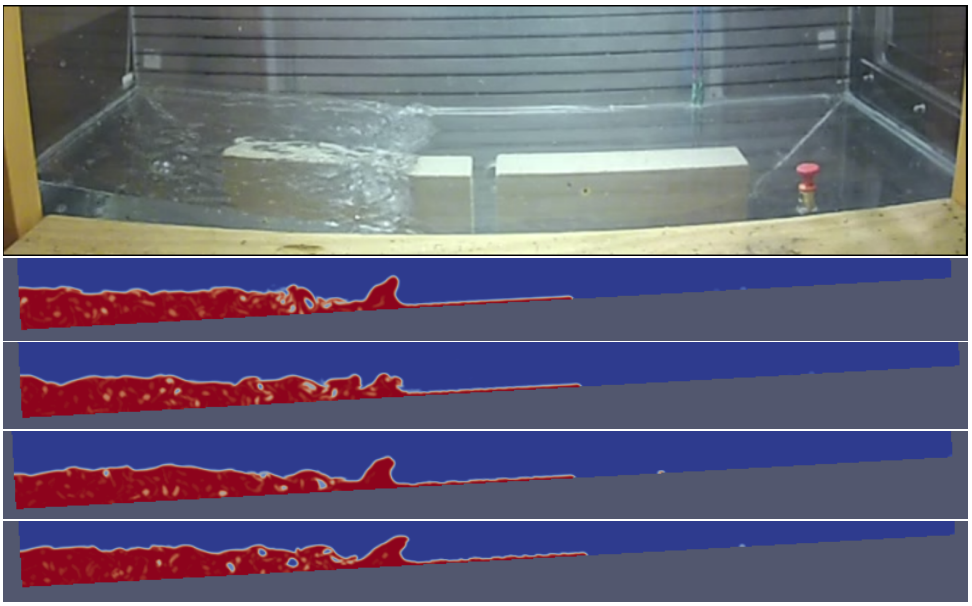

Figure 32: Images for tank test, S13, S14, S15 and S16 at t=3.9s

Lastly, for the free surface behaviour, the improvement is limited. Some of the fluid behaviour at the free surface is still unreal, i.e. at t = 3.15 s. Limited unphysical splashing exists in each case at the interface while the fluid motion in the tank test is very calm and mild soon after the first impact. Additionally, simulations S13 to S16 still slightly miss the second impact timing as in figure 33.

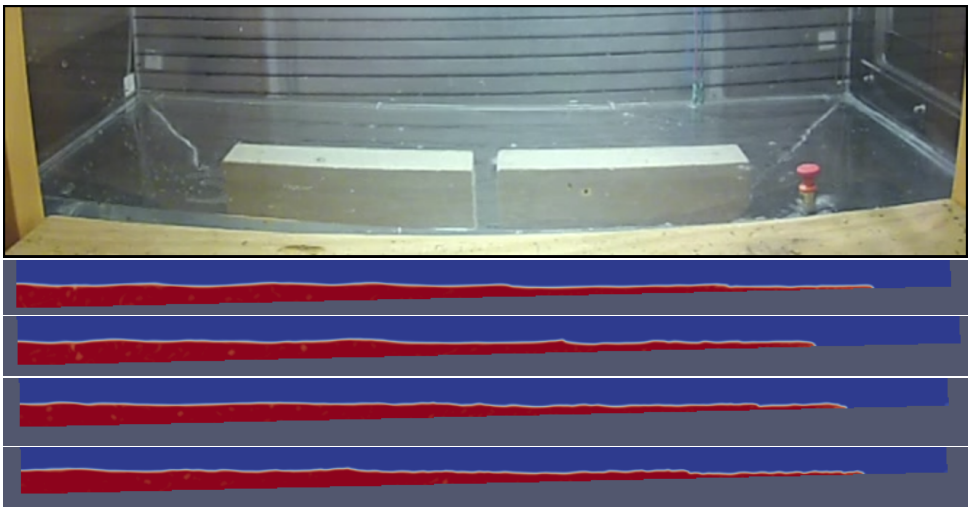

Figure 33: S13, S14, S15 and S16 miss the second impact time mark at t=5.4s

And as illustrated in figure 34, the moment history varied little. Nothing new stands out deserving further explained.

Basically, I tried to change cAlpha to see if there is significant diffusion in this sub-chapter. But the side effect is the appearance of significant ripples, and it becomes another new numerical error in the simulation. In cases S15 and S16 with cAlpha of 1.2 and 1.5, the ripples cannot be eliminated or decreased to an acceptable level. Meanwhile the solo wave at the bore still exists. As I cannot remove the unphysical solo wave phenomenon with high cAlpha values, whereas new error is bought in the simulation as the ripple, it is reasonable to exclude such high cAlpha values in the following simulation.

As S13 and S14 has acceptable simulation results in term of fluid motion details, there might be more effective solution with longer time step to save computational capacity. New time step is 0.002s for S17 and S18 with the same cAlpha values of S13 and S14. The appearance of the odd waves and its unphysical way of breaking, which is of great concern, exist as well. It proves time step as 0.002 s is not small enough. But further decreasing the time step below 0.001 s will require too much computational resources to fulfil the simulation. Hence in my case the optimal time step is 0.001 s as it is in S14.

In general, compared to 0.8 cAlpha value, 1.0 can make the simulation more close to the tank test under proper time step setting, which indicates that previously the simulation has certain diffusion problem that lead to some unphysical fluid behaviour such as the isolated noticeable wave on the hydraulic jump.

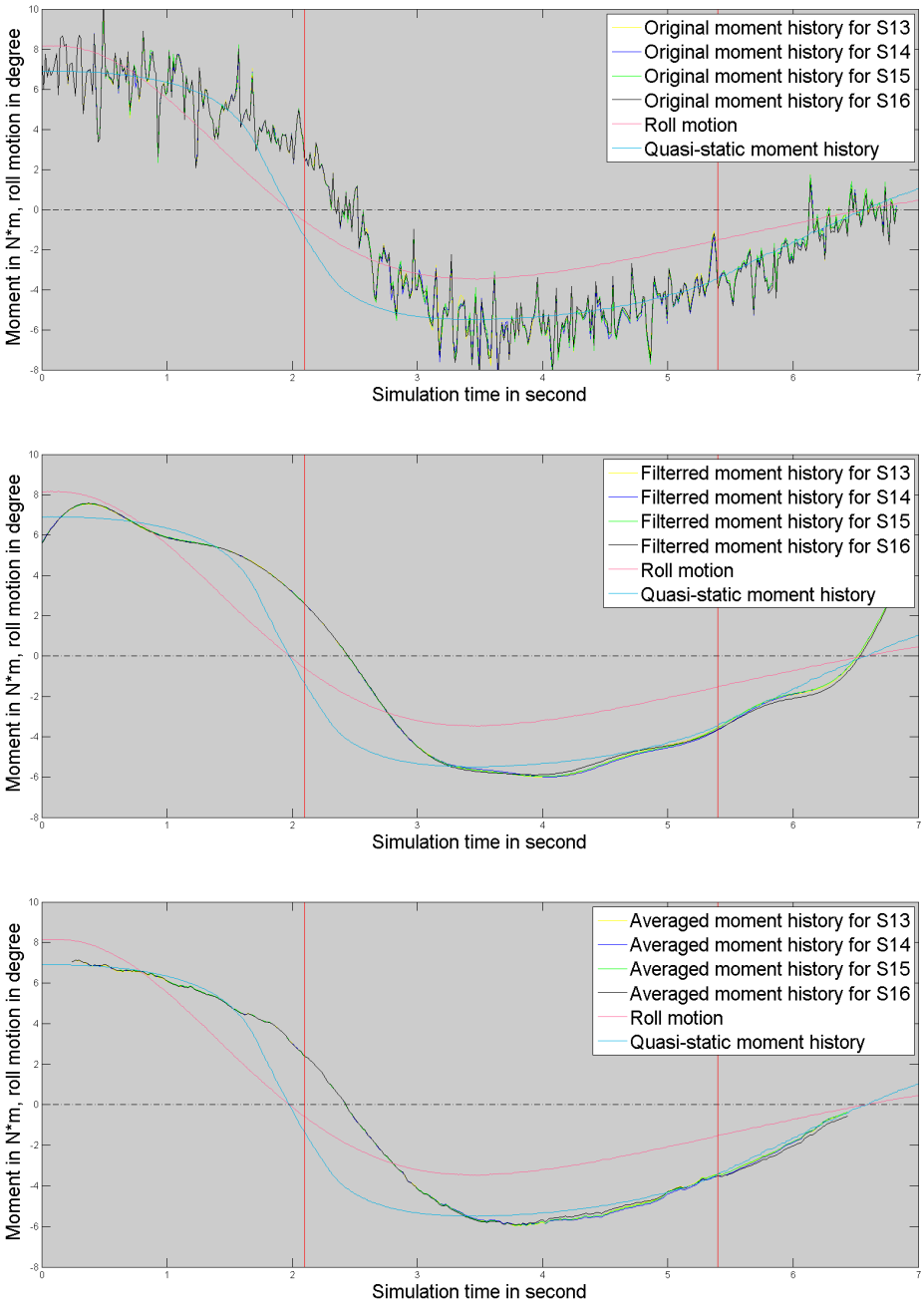

Figure 34: Original, filtered and averaged moment histories for S13, S14, S15 and S16

5 Analysis and summary

5.1 Key findings and analysis

During my simulations, the efforts focus on two main aspects: to refine sloshing moment history prediction and the fluid motion details. After the simulations, the final purpose is to study the damping effect of sloshing. So far, there have been some key findings related.

5.1.1 Sloshing water moment history

The attained sloshing moment prediction is good and dependable according to convergence and general fluid motion. In the convergence test, the sloshing moment history converges at a fairly coarse grid. Even grid as coarse as 320×32, where the cell size is around 2.5 mm$\times$2 mm, can provide a moment history that is very closed to that provided by the most refined grid S6 whose cell size is 0.5 mm$\times$ 0.5 mm. Therefore, all the grids that are applied in the simulations are supposed to have converged. Besides, their general fluid motion and impact time marks match with the tank test very well, which can be proved by the image comparison in the Appendix A. Though there are some incorrect phenomenon such as excessive trapped air in the simulations, they do not harm the accuracy of the sloshing moment prediction. The reason is that the phenomenon is related to hydrodynamic forces. As it is a free decaying roll motion with limited amplitude, there is neither resonance nor violent oscillation. The amplitude of sloshing water is trivial. Therefore the hydrodynamic pressure is of little importance considering its small impact. Meanwhile, most of the bottom area is pressured by the hydrostatic forces, and water is moving from side to side. Hence, the hydrostatic pressure plays a very crucial role in the exerted moment on the tank due to its magnitude and the relatively long arm . And as mentioned, the general fluid motion is well simulated, which is tightly related to the hydrostatic forces. Therefore, the sloshing moment prediction is robust and reliable. In the perspective of dependable moment prediction and fast simulation, the setting of S7 is adequate and recommended.

5.1.2 Simulation details of the sloshing water motion

To physically simulate all the details of the fluid motion difficult task. The main barriers are the trapped air in the water and unreal phenomena at the free surface including violent splashing and isolated wave at the bore.

Adding the surface tension can greatly improve the simulation in term of trapped air and part of the unreal interface phenomenon. Air bubbles inside the water float to the free surface at a much faster speed, which is more reasonable. It also makes less air get trapped, and the trapped air is easier to form larger bubbles. They no longer stationarily stay in water. Furthermore, it helps decrease the violent interaction of water at the interface. With surface tension added, there remains only limited unphysical splashing, though it is not totally shut down. But surface tension does not help diminish the odd solo wave at the bore, which is a false water motion due

to diffusion. Taking proper time step and cAlpha value can effectively decrease the height of the wave due to decreased diffusion.

During the convergence test and the study of diffusion problem, it can be generalized that the appearance of ripples is linked to the non-square cells and large cAlpha value. Backward time scheme can also cause severe ripples. The problem triggered by non-square cells is linked with VOF principle. When the width of the cell is shorter than its height, the interface in the cell may probably be more compressed in horizontal direction than in vertical direction. So the small waves can be compressed into spikes or shape ripples in figure 20. For cAlpha, it is the artificial coefficient that makes the interface more compact and thinner. A large cAlpha can lead to ripples due to overcompression. Evidences are the images of S10 to S16 as shown in Appendix C and D. Besides, as a result, reducing time step can hardly limit the generation of ripples.

At last, decreasing diffusion in the simulation as much as possible can diminish some unreal interface phenomenon. After multiple tests, when cAlpha is 1.0 at certain time step setting, diffusion is likely to be diminished to a satisfied level. Reducing time step cannot solve the ripples problem, but it certainly does refine the quality of simulation, which has been explained in Section 3.1. The smaller time step is, the more frequently fluid properties is updated during the simulation. Therefore based on the refined simulation quality, increased cAlpha can decrease the diffusion without much side-effect such as ripples.

On thing needs to be specified is that OpenFOAM cannot realize free slip conditon on all the boundaries, since it cannot handle ship boundary with motion in the normal direction to the boundary.

Conclusively, by using square cells while simulating and choosing proper cAlpha under time step that is short enough, the interface behaviour is refined greatly and it is fairly closed to the images of the experiment. At last, anyway there are still excessive entrapped air and uphysical interface behaviour. But, they are limited and acceptable in the end after improvement. In this work, compared with other simulations, S14 is recommended.

5.1.3 Damping effect by sloshing

Basing on the sloshing moment, it is possible to study its damping effect. By comparing it to the roll motion and quasi-static moment in figure 34, obviously the sloshing moment lags behind the roll motion. Since the tank motion is transient and decaying, so there is no so-called period in my case. In the time domain and based on S14, the sloshing water damps the tank motion in the period from 0 to around 2.4 s and the period between t = 3.5 s and t = 6.5 s. From about t = 2.4 s to t = 3.5 s and after t = 6.5 s, the sloshing water accelerates the tank motion. The sloshing moment history lags behind the quasi-static moment history with about 0.5 s at the first impact. But it almost catches the quasi-static moment history at the second impact. In the perspective of energy. The water gains the kinematic energy from the tank motion through interaction, and the roll motion is decaying with a decreasing amplitude. During the interaction with tank motion, namely the impacts, kinematic

energy of fluid keeps dissipating. The energy is transmitting to heat. Meanwhile the water also regains energy from the collision with the tank. But as mentioned, the roll motion amplitude keep declining, therefore the energy the fluid can receive is not enough to keep it moving with the same amplitude of its previous motion. Correspondingly, fluid motion is decaying, meaning the amplitude of hydraulic jump declines, meaning the free surface is gradually becoming flat and horizontal, meaning its behaviour and exerting moment is approaching the quasi-static motion, and so is its moment. Generally speaking, the sloshing moment damps the tank motion since it draws energy from the tank and dissipates it. However, it accelerates the roll motion within certain period, which is adverse for naval architecture stability and should be avoided while designing. Attention should be paid that the low-pass filtering method may have certain problem as we can see the sloshing moment, i.e, in figure 34, goes unexpectedly high after the second impact, and it does not match with the original moment history at this period.

5.2 Potential improvement & further work

After a series of simulation tests, some experience and understanding are acquired. Here also comes out some thoughts about the potential to improve the simulation.

3D effect is a crucial factor that should be taken into account. Firstly, it influences the motion of the air trapped as mentioned previously. In 2D condition, once there is air trapped into the water, the generated bubble will float and penetrate the whole free surface in the longitudinal X-direction. However, if it is simulated in 3D, probably it will be observed that some bubbles might get together to form a bigger bubble and then float to penetrate only certain part of the free surface in X-direction. Also, some bubbles might break into smaller bubbles due to pressure. These are possible reasons to make the simulated interface behaviour smoother and get rid of the excessive water splashing.

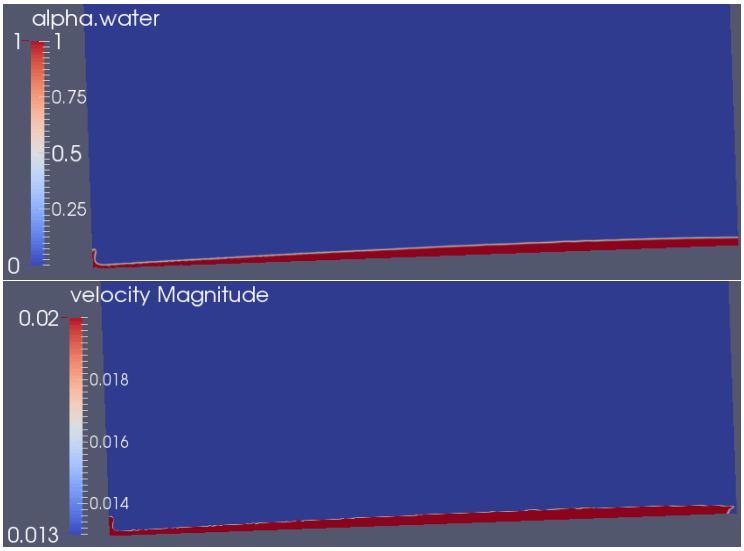

Figure 35: Fluid motion and velocity contour plot of S14

In addition, my case is simulated as a laminar problem. To stay out of turbulence flow regime, Re needs to be below 10^4, which makes the fluid velocity in my case under 0.013 m/s. From figure 35, it can be found that the velocity are always above 0.013 m/s. In other words, the fluid motion is in turbulence. Thus, simply defining this model as laminar might lead to ignoring some important fluid characteristics while simulating.

And lastly, reducing time step is another potential method to improve the simulation, whereas it will also require much more powerful computational capacity.

Due to the limitation of computational capacity, 3D model and reducing time step further are not realistic. And establishing turbulence model is a very complex work and requires much work and time which is not affordable. But this can be left for further development in the future to complete this study.

5.3 Conclusion

The goal of this thesis work is to simulate and study shallow water sloshing and its damping effect. OpenFOAM CFD method provides qualitatively and quantitatively good result for the moment prediction. Due to the limited roll motion, the hydrodynamic moment become quite insignificant to the total sloshing moment. This lowers the difficulty to yield reliable sloshing moment prediction from the simulation because it allows me to omit some physical sloshing details that I fail to simulate. In this point of view, the attained sloshing moment histories are trustworthy, and the most efficient simulation is S7.

As for the sloshing phenomenon details, in S14, the simulation of the interface behaviour now is acceptable though there still remain some unphysical phenomena. The excessive trapped bubbles due to air-fluid interaction are not totally solved yet, even though this phenomenon in simulation has been refined quite a lot. In general, most of the sloshing fluid motion has been well simulated. Only some details are failed to represent in the simulation. The best simulation so far is S14, and to further improve the quality, more computation resources and time are needed.

The sloshing water shows damping effect and accelerating effect to the free decaying tank motion from period to period, but generally it induces damping effect on the transient tank motion. Thus, in fact, the shallow water sloshing has an positive effect on the ship stability in transient motion. Since this case is what Lumped Mass method[14] fails to predict in terms of the sloshing moment, this work can hopefully provide some ideas and information to further develop the method so that calculation of the ship stability would be more quick, simple and accurate. And also, it helps to understand the shallow water sloshing better, especially with a transient tank motion.

References

[1] J. A. Alsgaard. Numerical investigation of piston mode resonance in a moon-pool using openfoam. Master's thesis, Norwegian University of Science andv Technology, 2010.

[2] A. B. Biran. *Ship Hydrostatics and Stability*. Elsevier Ltd., 2003.

[3] D. E. Elger. Experimental investigation of the superposition principle for a free surface roll damping tank. Master's thesis, Norwegian University of Science and Technology, 2014.

[4] Odd M. Faltinsen and Alexander N. Timokha. *Sloshing*. Cambridge University Press, 2009.

[5] J. H. Ferziger and M. Peric. *Computational Methods for Fluid Dynamics*. Springer-Verlag, 1999.

[6] C. A. J. Fletcher. *Computational Techniques for Fluid Dynamics*. Springer-Verlag, 1991.

[7] J. Gomez-Goni, C. A. Garrido-Mendoza, J. L. Cercos, and L. Gonzalez. Two phase analysis of sloshing in a rectangular container with volume of fluid methods. *Ocean Engineering*, 2013.

[8] C. Hirsch. *NUMERICAL COMPUTATION of INTEGRAL and EXTERNAL FLOWS*, volume 2. John Wiley & Sons, Inc, 1990.

[9] C. W. Hirt and B. D. Nichols. Volume of fluid(vof) method for the dynamics of free boundaries. *JOURNAL OF COMPUTATIONAL PHYSICS*, 39:201–225, 1981.

[10] E. Kreyszig. *Advanced engineering mathematics*. John Wiley & Sons, Inc, 1999.

[11] E. V. Lewis, editor. *Princeples of Nval Architecture*, volume 3. The Society of Naval Architecture and Marine Engineers, 1989.

[12] G. R. Liu and M. B. Liu. *Smoothed Particle Hydrodynamics-a meshfree particle method*. World Scientifi Publishing Co. Pte. Ltd., 2003.

[13] T. Manderbacka, P. Ruponen, J. Kulovesi, and J. Matusiak. Model experiments of the transient response to floolding of the box shaped barge. *Journal of Fluids and Structures*, 2015.

[14] T. L. Manderbacka, T. K. Mikkola, and J. E. Matusiak. Study of damping effect of the floodwater on a damaged ship rool motion. *Accepted to: Proceedings of the ISOPE-2015 25th International Offshore and Polar Engineering Conference, Kona, Hawaii, USA*, 2015.

[15] G. CJ. Morgan. *APPLICATION OF THE INTERFOAM VOF CODE TO COASTAL WAVE/STRUCTURE INTERACTION*. PhD thesis, University of Bath, 2013.

[16] O. Rognebakke. *Sloshing in rectangular tanks and interaction with ship motions*. PhD thesis, Nowegian University of Science and Technology, 2002.

[17] H. Rusche. *COMPUTATIONAL FLUID DYNAMICS OF DISPERSED TWO-PHASE FLOWS AT HIGH PHASE FRACTIONS*. PhD thesis, Imperial College of Science, Technology and Medicine, 2002.

[18] Jiyuan Tu, Guan Heng Yeoh, and Chaoqun Liu. *Computational fluid dynamics: a practical approach*. Butterworth-Heinemann, 2008.

[19] J. H. G. Verhagen and L. Van Wijngaarden. Non-linear oscillations of fluid in a container. *J. Fluid Mech.*, 22:737–751, 1965.

[20] H. K. Versteeg and W. Malalasekera. *An Introduction to COMPUTATIONAL FLUID DYNAMICS-The Finite Volume Method*. Prentice Hall, 2007.

[21] J. H. Vugts. A comparative study on four different passive roll damping tank, part 1. Technical report, Netherlands Ship Research Centre TNO, 1968.

[22] F. M. White. *Fluid Mechanics*. William C Brown pub, 1998.

A Appendix A

The following is the image comparison among tank test, S1, S2, S4[1], S5 and S6.

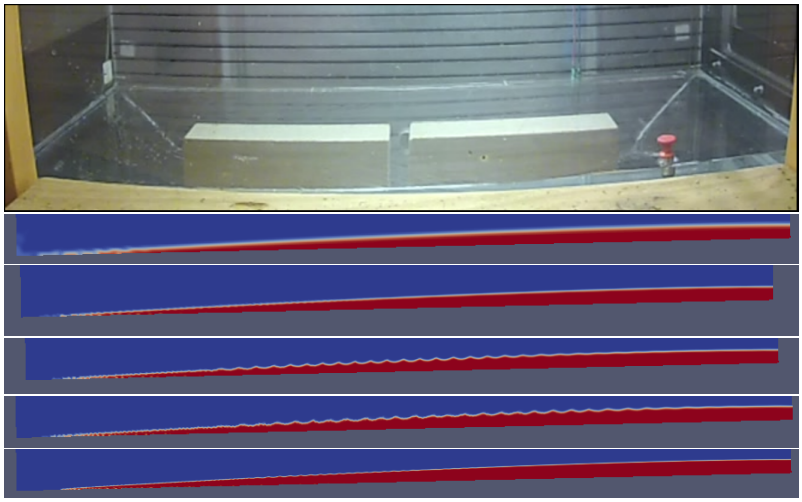

Figure A1: Images for tank test and simulations with mesh densities of 320×32, 800×70, 1000×70, 1200×70 and 1400×140 at t=2.4s

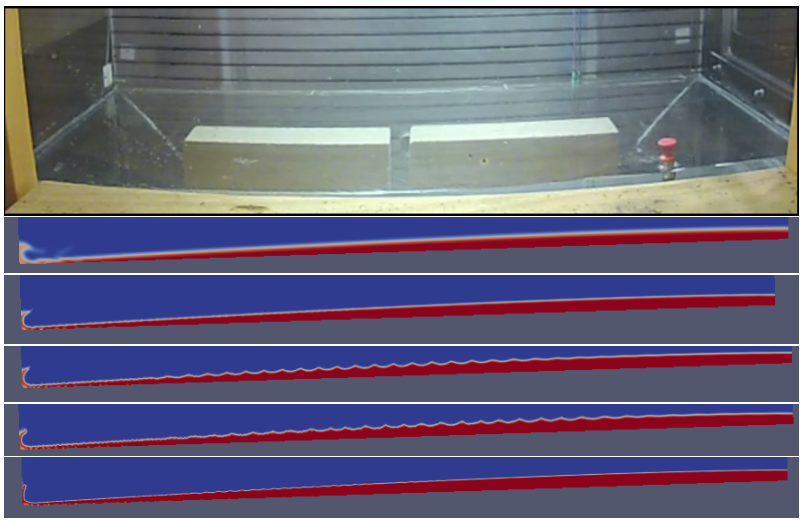

Figure A2: Images for tank test and simulations with mesh densities of 320×32, 800×70, 1000×70, 1200×70 and 1400×140 at t=2.4s

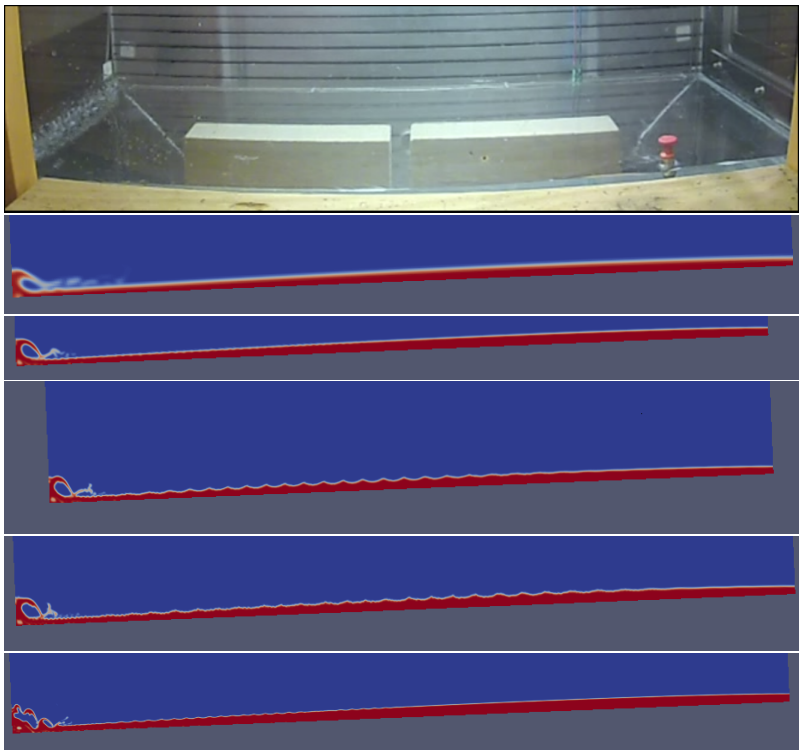

Figure A3: Images for tank test and simulations with mesh densities of 320×32, 800×70, 1000×70, 1200×70 and 1400×140 at t=2.4s

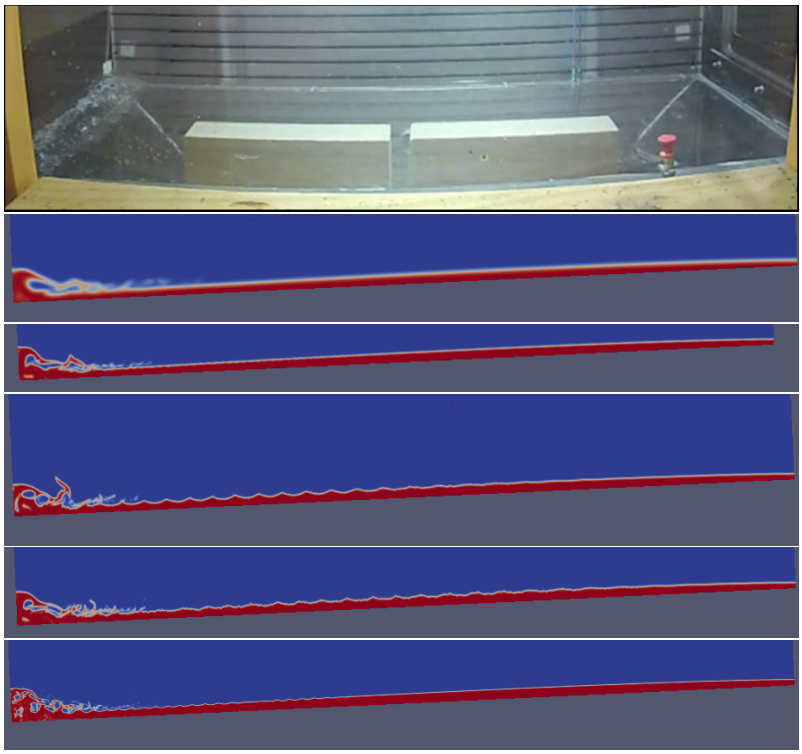

Figure A4: Images for tank test and simulations with mesh densities of 320×32, 800×70, 1000×70, 1200×70 and 1400×140 at t=2.55s

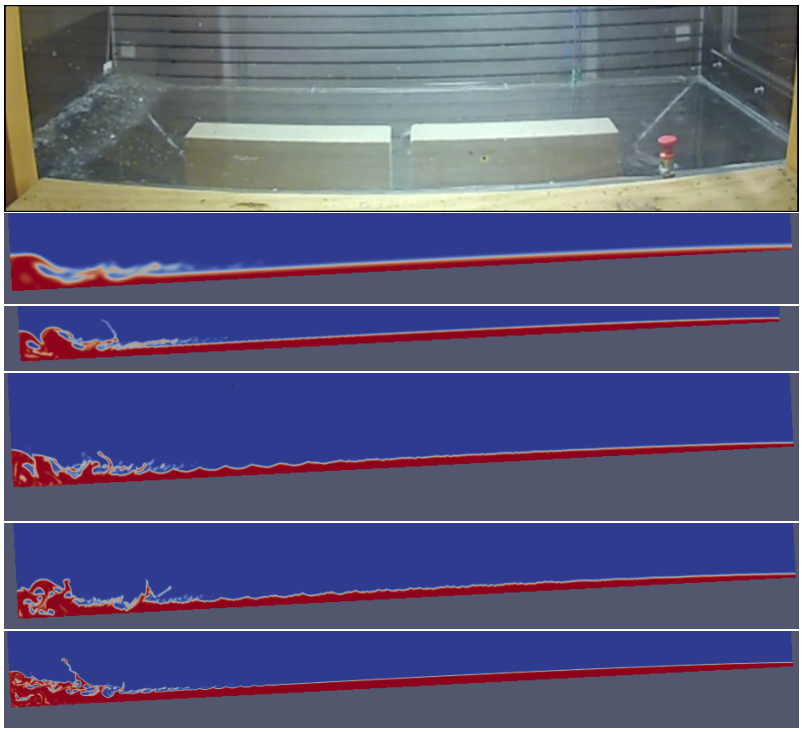

Figure A5: Images for tank test and simulations with mesh densities of 320×32, 800×70, 1000×70, 1200×70 and 1400×140 at t=2.7s

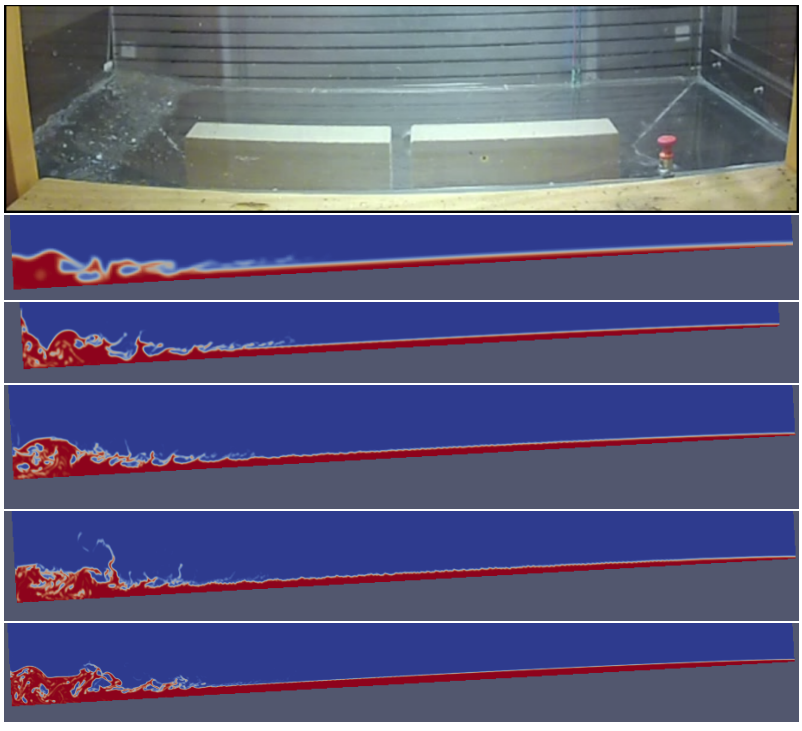

Figure A6: Images for tank test and simulations with mesh densities of 320×32, 800×70, 1000×70, 1200×70 and 1400×140 at t=2.85s

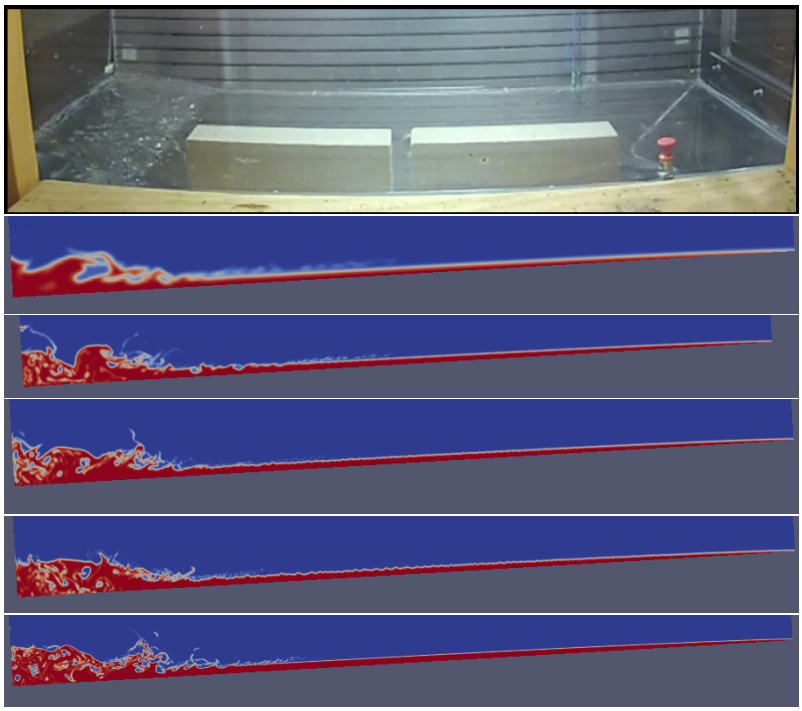

Figure A7: Images for tank test and simulations with mesh densities of 320×32, 800×70, 1000×70, 1200×70 and 1400×140 at t=3s

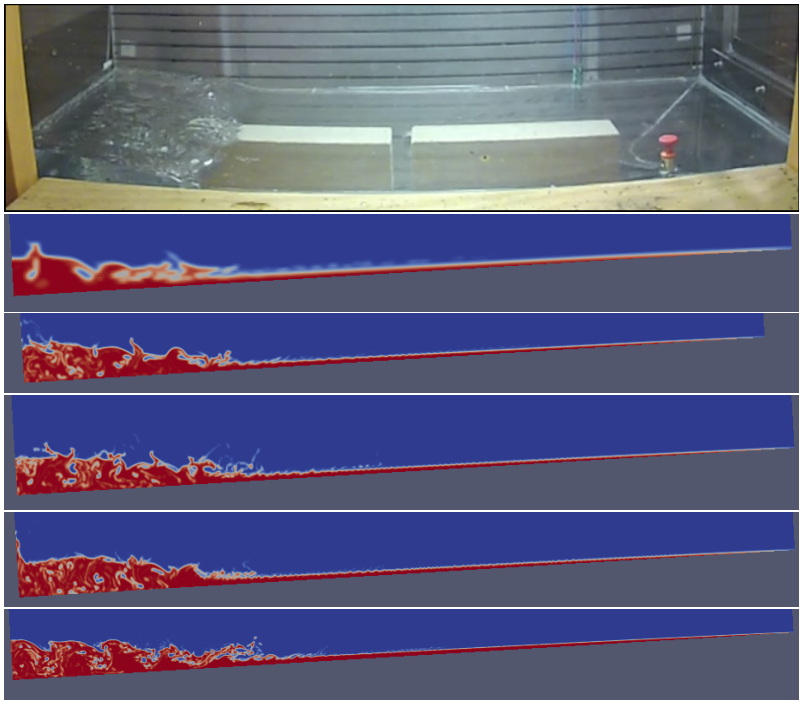

Figure A8: Images for tank test and simulations with mesh densities of 320×32, 800×70, 1000×70, 1200×70 and 1400×140 at t=3.3s

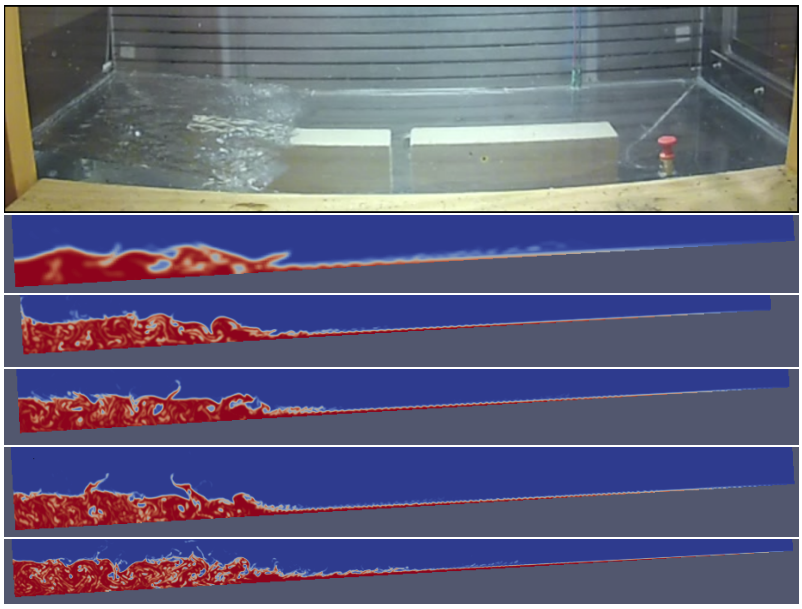

Figure A9: Images for tank test and simulations with mesh densities of 320×32, 800×70, 1000×70, 1200×70 and 1400×140 at t=3.6s

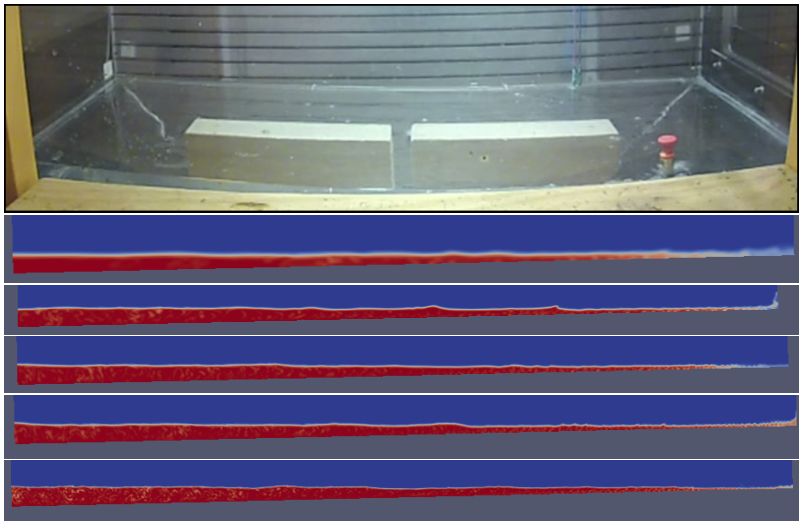

Figure A10: Images for tank test and simulations with mesh densities of 320×32, 800×70, 1000×70, 1200×70 and 1400×140 at t=5.4s

B Appendix B

Interface image comparison among tank test, S1, S7, S8 and S9.

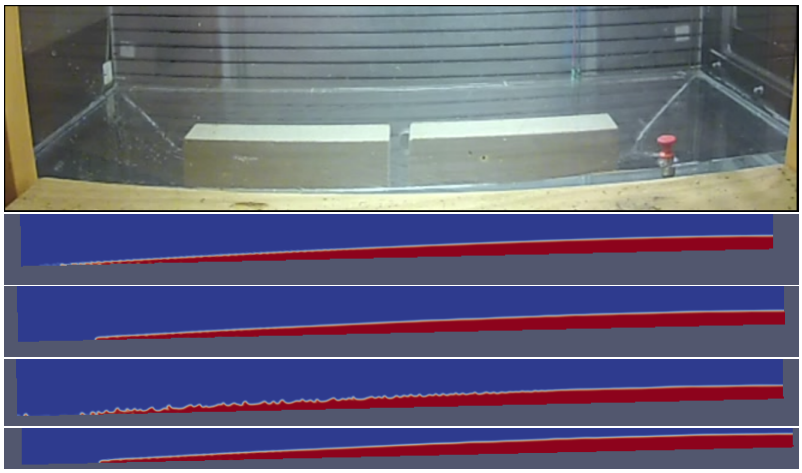

Figure B1: Images for tank test, S1, S7, S8 and S9 at t = 2.1 s

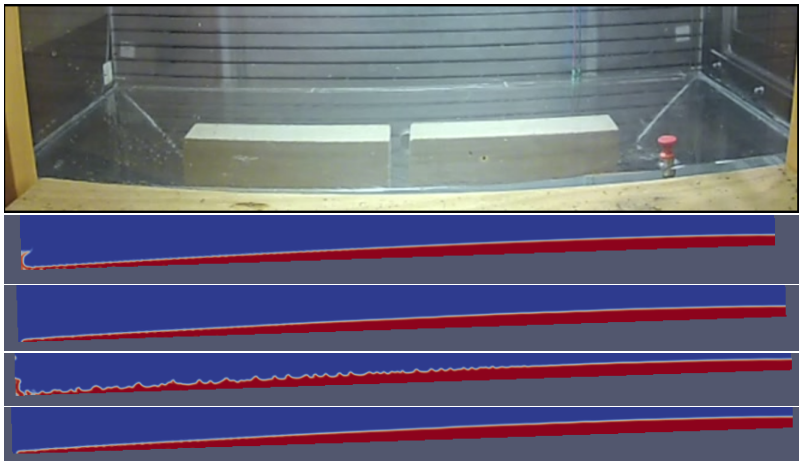

Figure B2: Images for tank test, S1, S7, S8 and S9 at t = 2.25 s

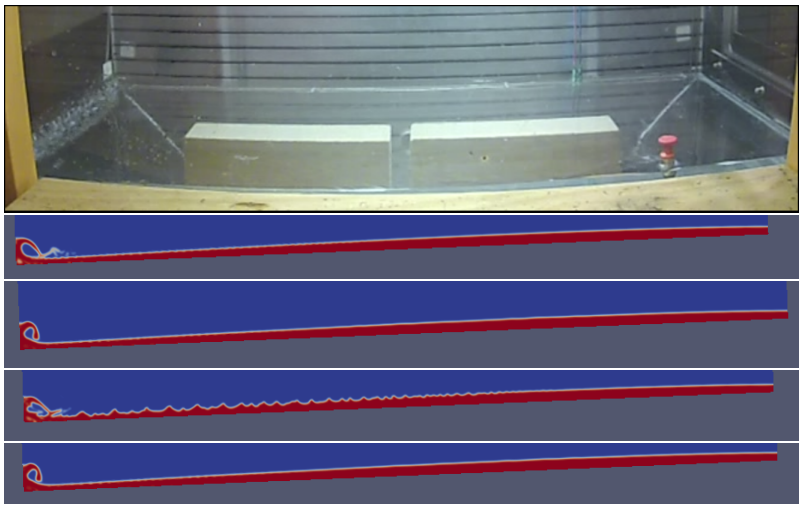

Figure B3: Images for tank test, S1, S7, S8 and S9 at t = 2.4 s

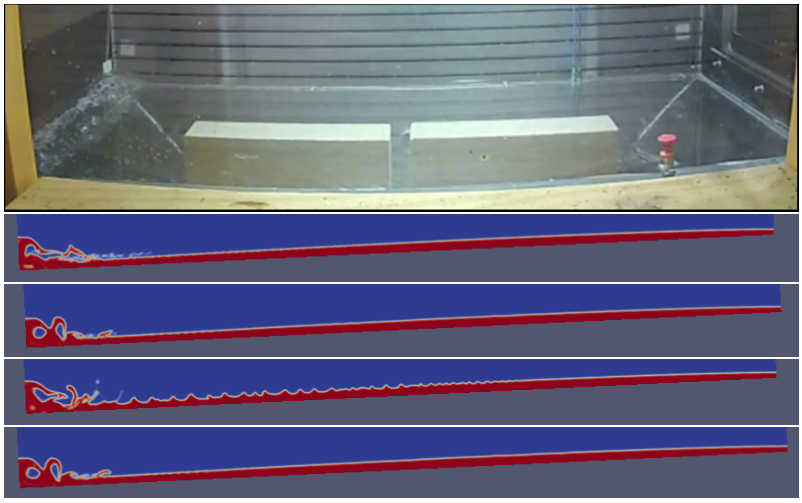

Figure B4: Images for tank test, S1, S7, S8 and S9 at t = 2.55 s

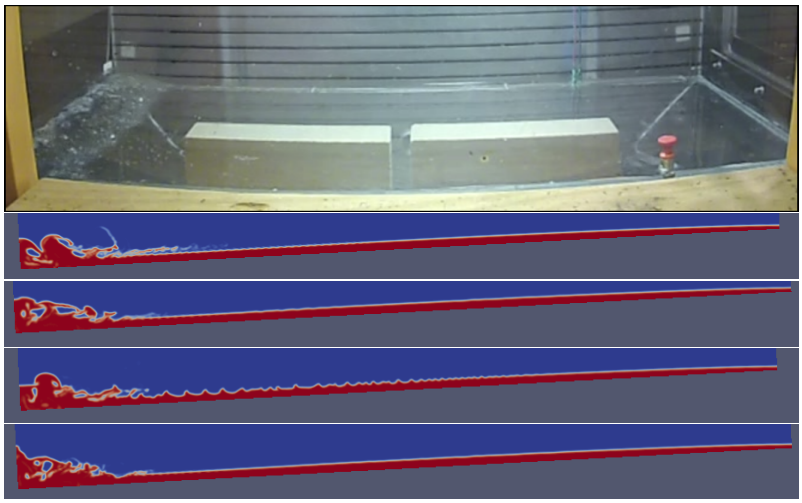

Figure B5: Images for tank test, S1, S7, S8 and S9 at t = 2.7 s

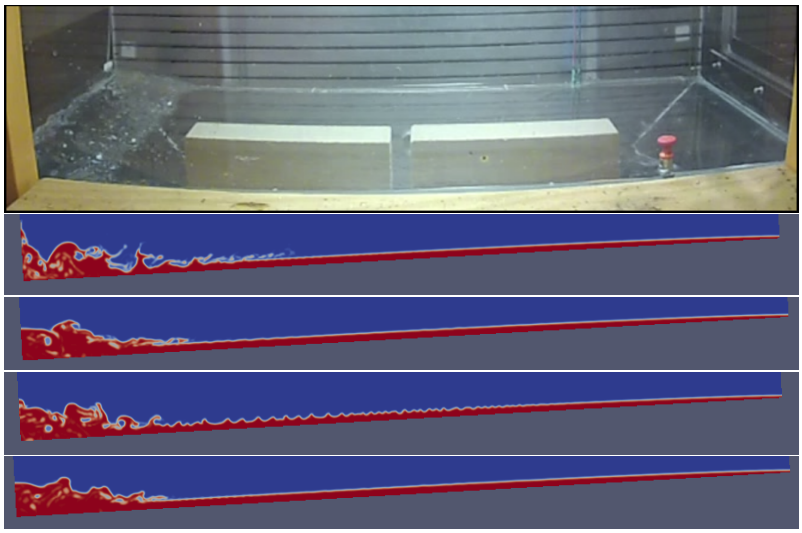

Figure B6: Images for tank test, S1, S7, S8 and S9 at t = 2.85 s

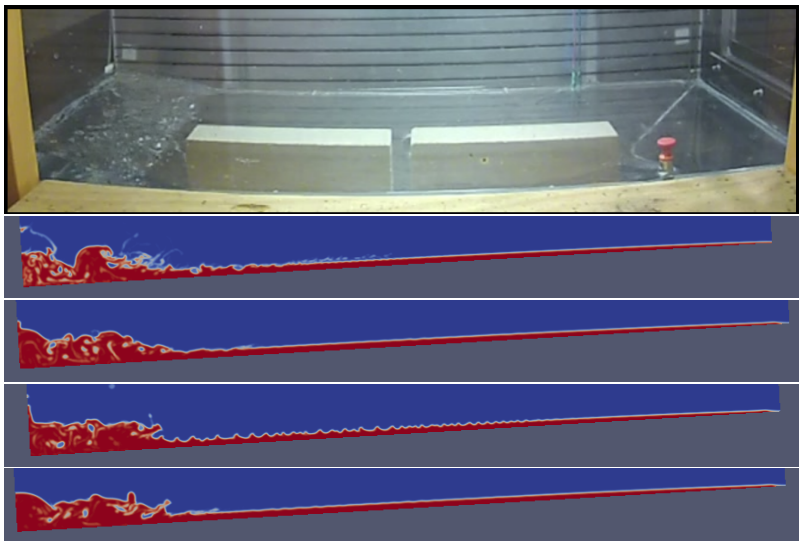

Figure B7: Images for tank test, S1, S7, S8 and S9 at t = 3.0 s

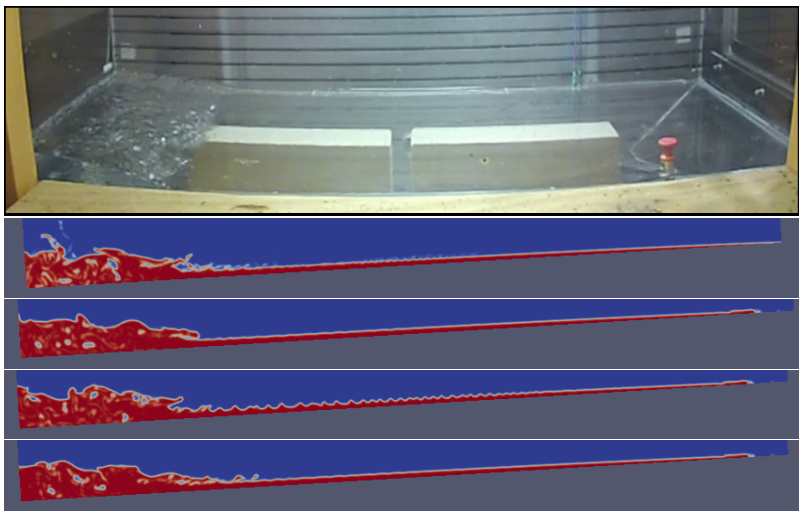

Figure B8: Images for tank test, S1, S7, S8 and S9 at t = 3.15 s

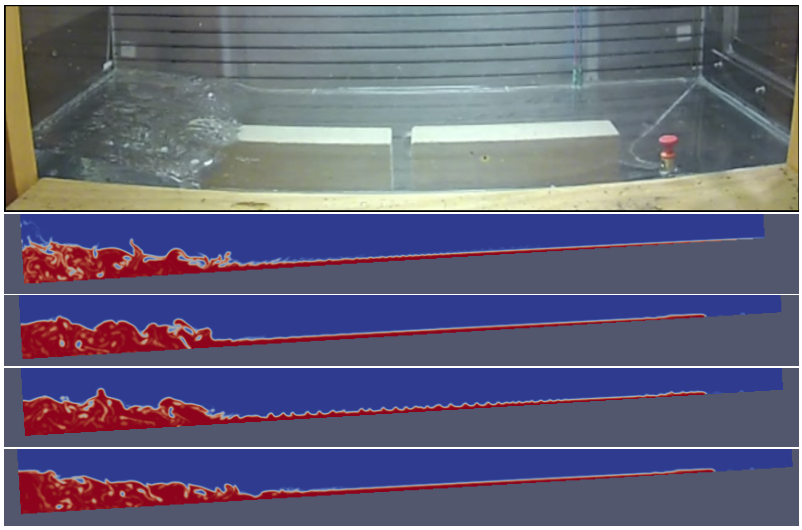

Figure B9: Images for tank test, S1, S7, S8 and S9 at t = 3.3 s

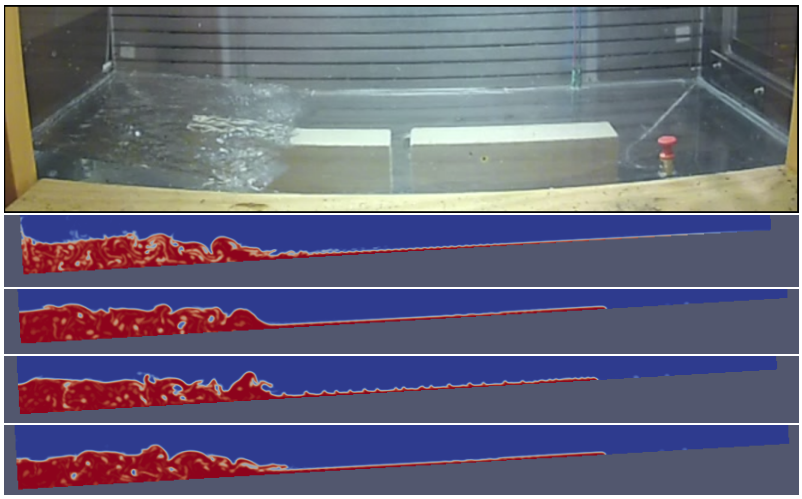

Figure B10: Images for tank test, S1, S7, S8 and S9 at t = 3.6 s

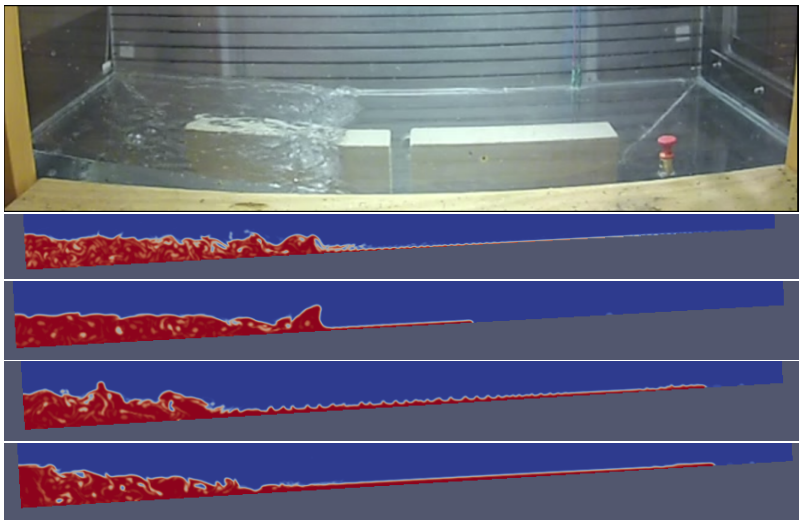

Figure B11: Images for tank test S1 and S7 at t = 3.9 s

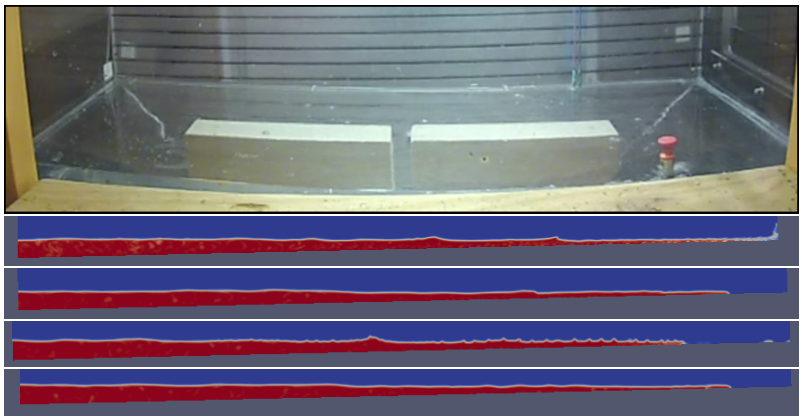

Figure B12: Images for tank test, S1, S7, S8 and S9 at t = 5.4 s

C Appendix C

The following are the image comparison among the tank test with S7, S10, S11 and S12.

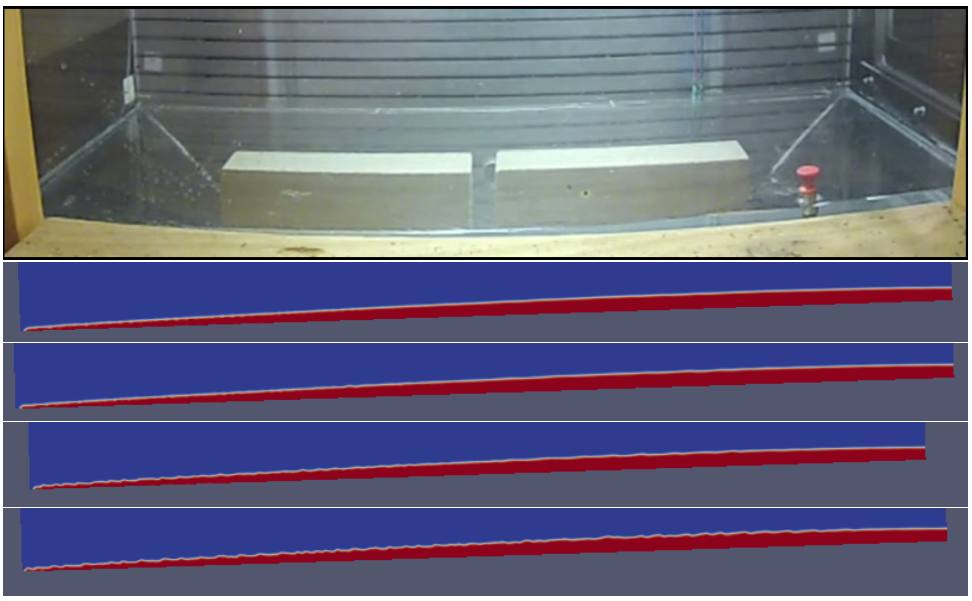

Figure C1: Images for tank test and S7, S10, S11 and S12 at t=2.25s

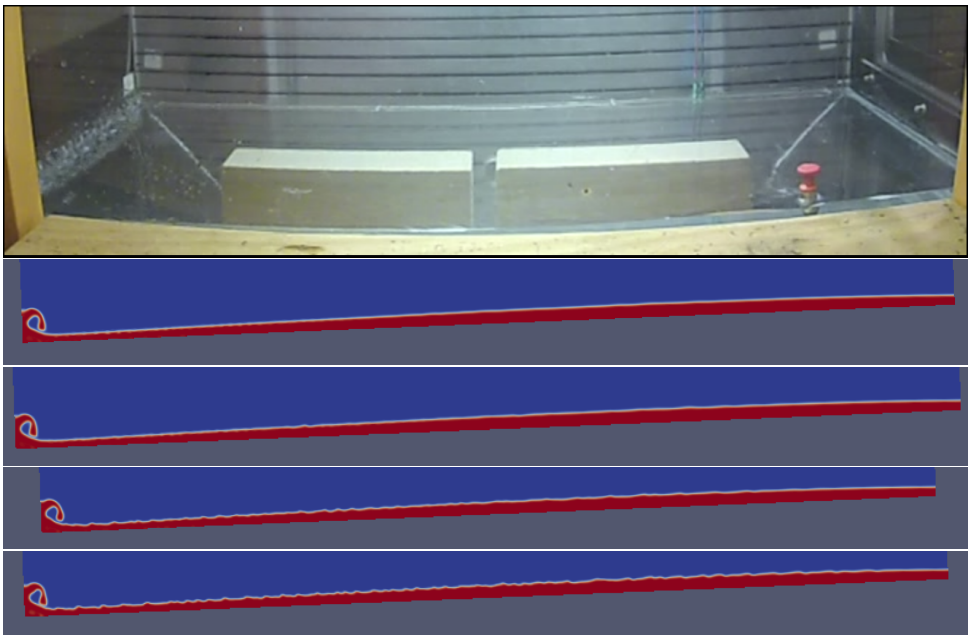

Figure C2: Images for tank test and S7, S10, S11 and S12 at t=2.4s

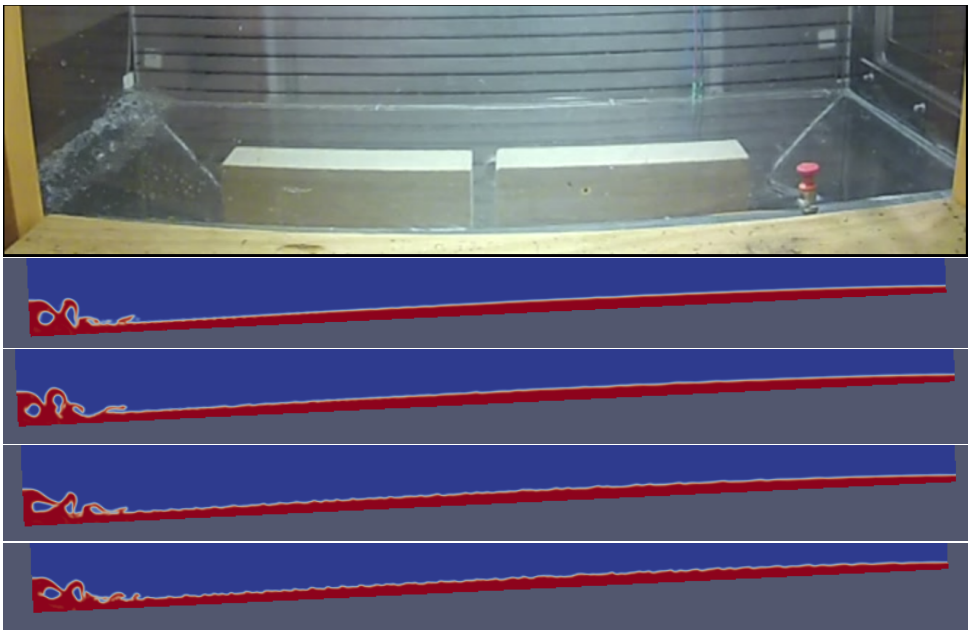

Figure C3: Images for tank test and S7, S10, S11 and S12 at t=2.55s

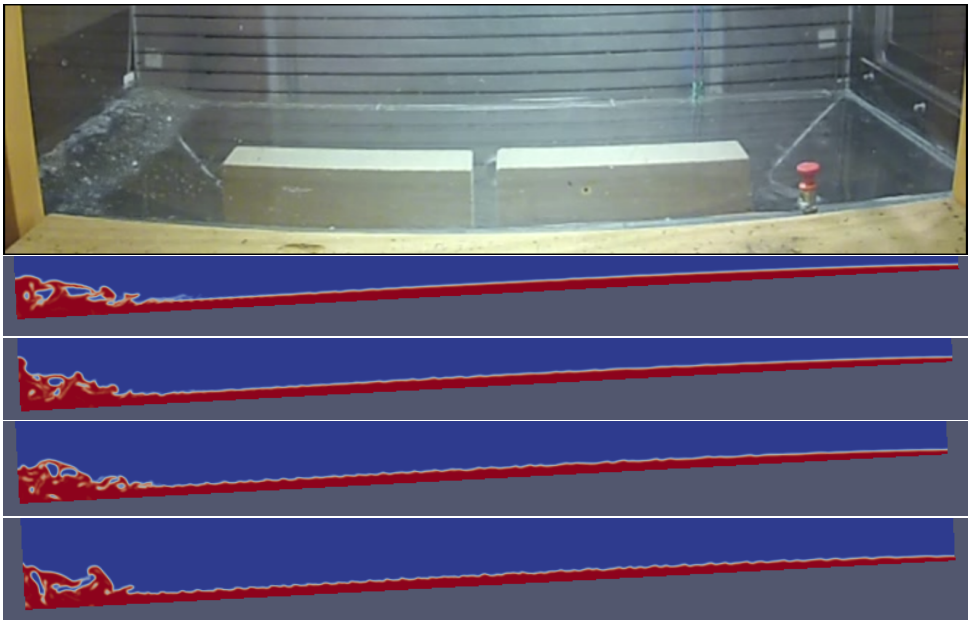

Figure C4: Images for tank test and S7, S10, S11 and S12 at t=2.7s

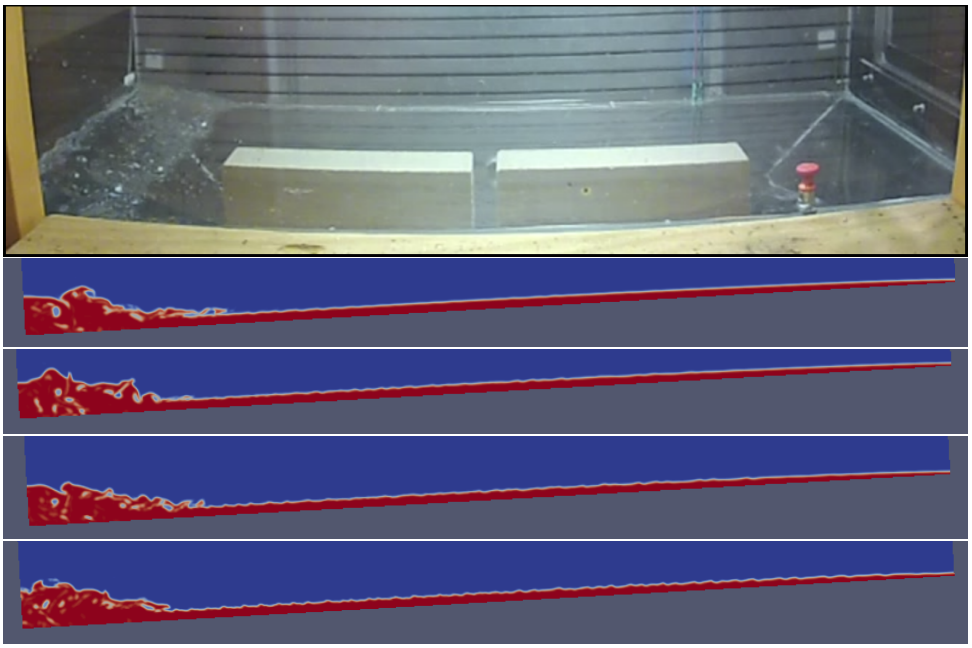

Figure C5: Images for tank test and S7, S10, S11 and S12 at t=2.85s

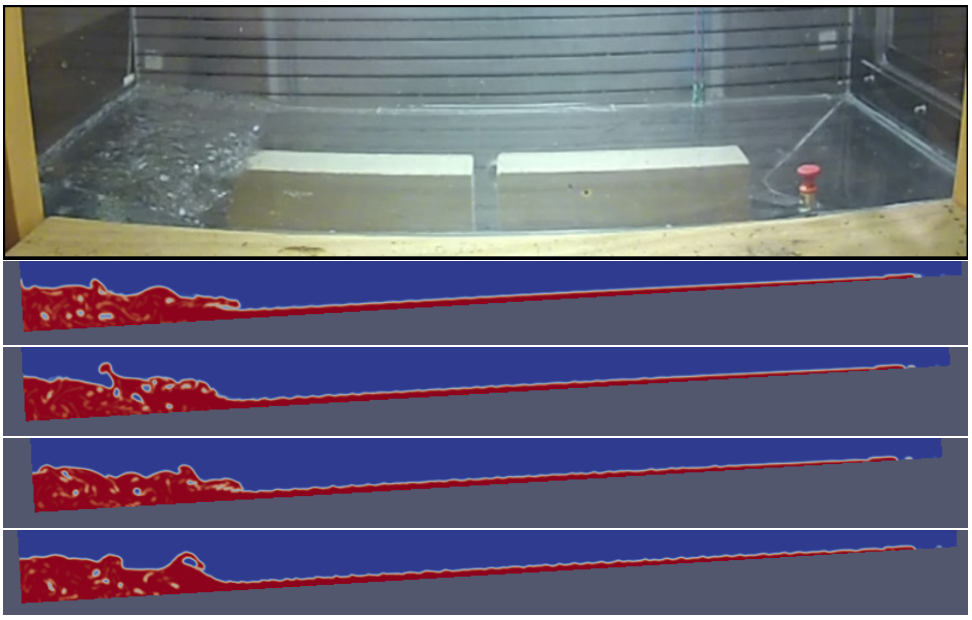

Figure C6: Images for tank test and S7, S10, S11 and S12 at t=3.15s

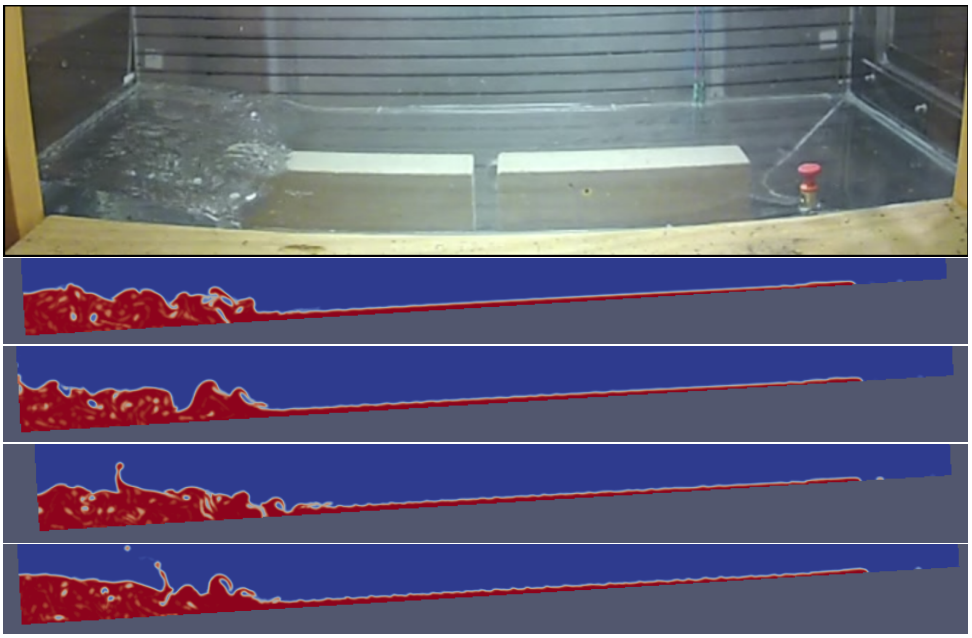

Figure C7: Images for tank test and S7, S10, S11 and S12 at t=3.3s

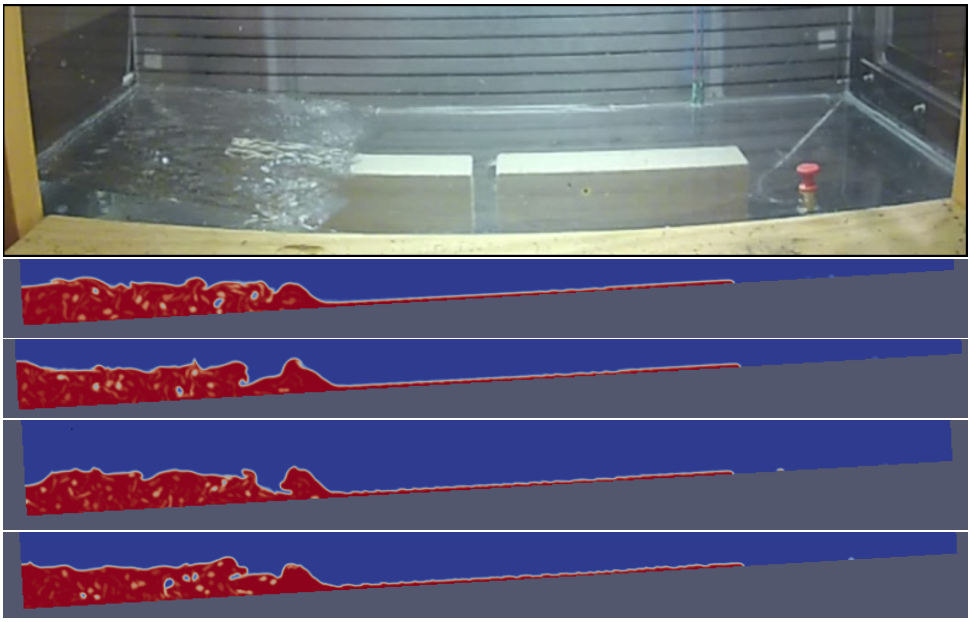

Figure C8: Images for tank test and S7, S10, S11 and S12 at t=3.6s

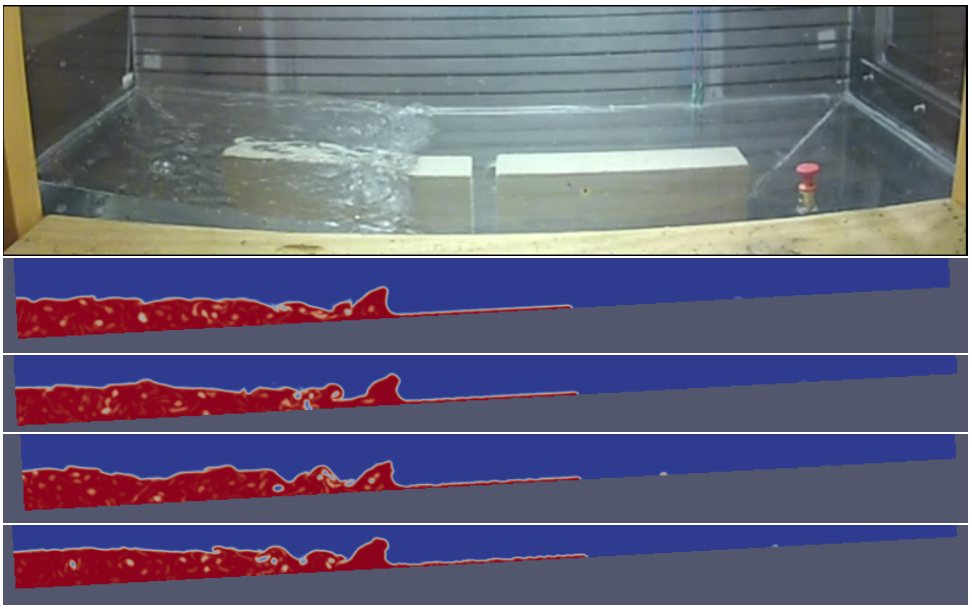

Figure C9: Images for tank test and S7, S10, S11 and S12 at t=3.9s

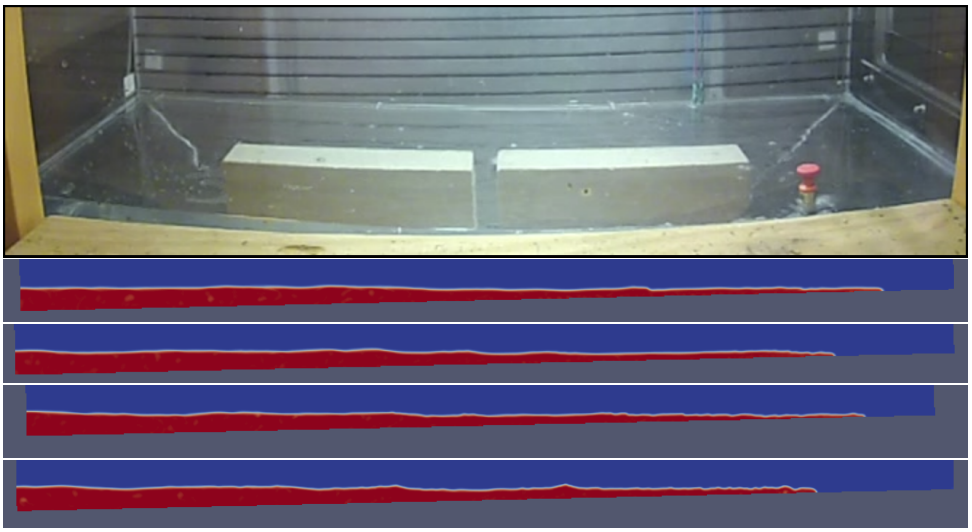

Figure C10: Images for tank test and S7, S10, S11 and S12 at t=5.4s

D Appendix D

Figures below are the image comparison among the tank test with S13, S14, S15 and S16.

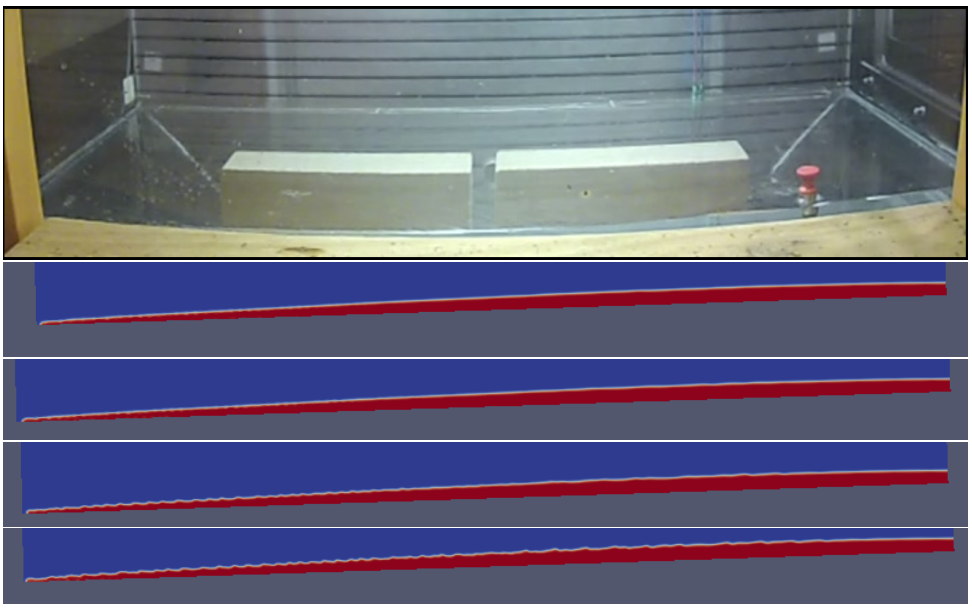

Figure D1: Images for tank test, S13, S14, S15 and S16 at t=2.25s

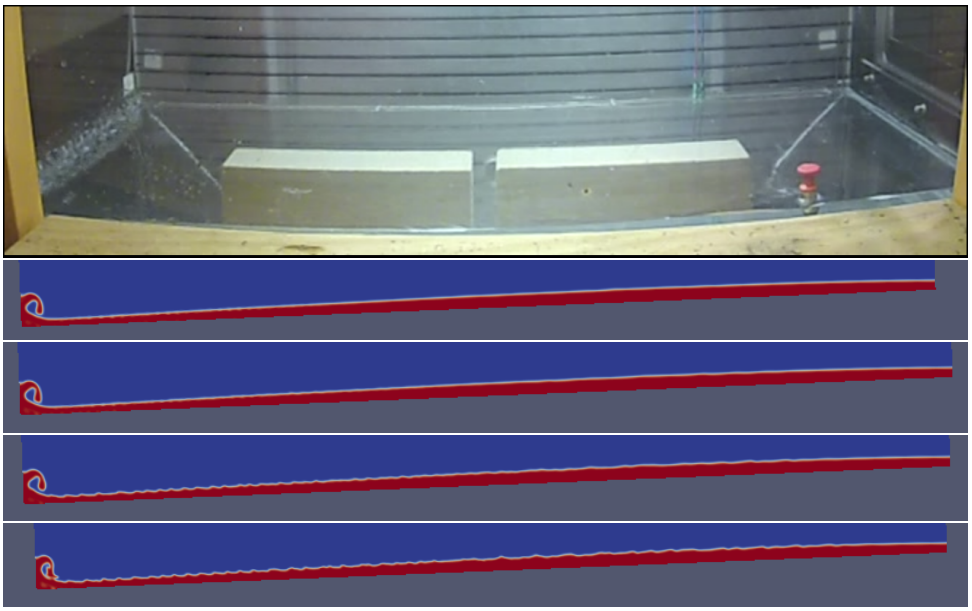

Figure D2: Images for tank test, S13, S14, S15 and S16 at t=2.4s

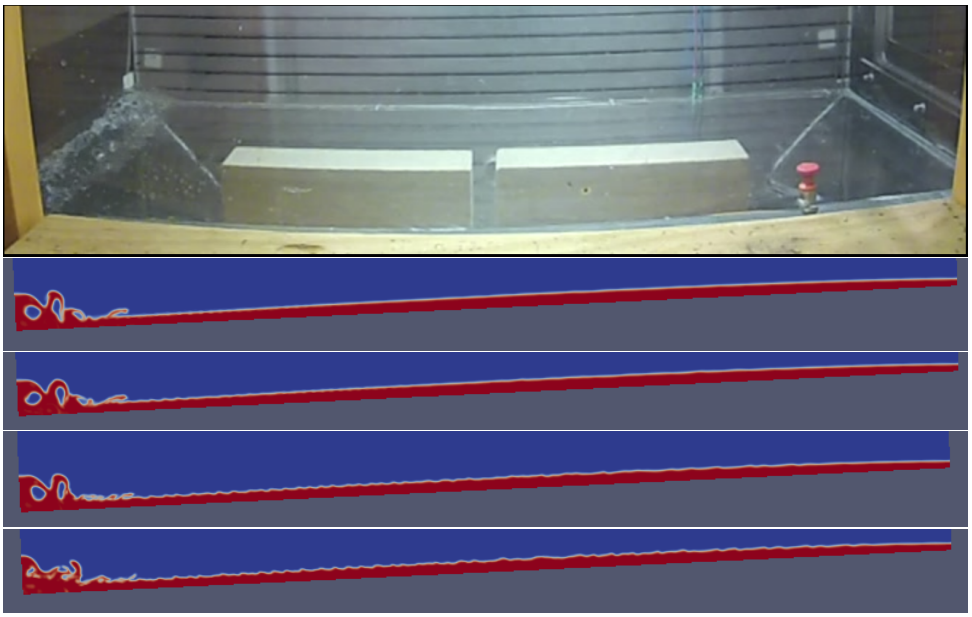

Figure D3: Images for tank test, S13, S14, S15 and S16 at t=2.55s

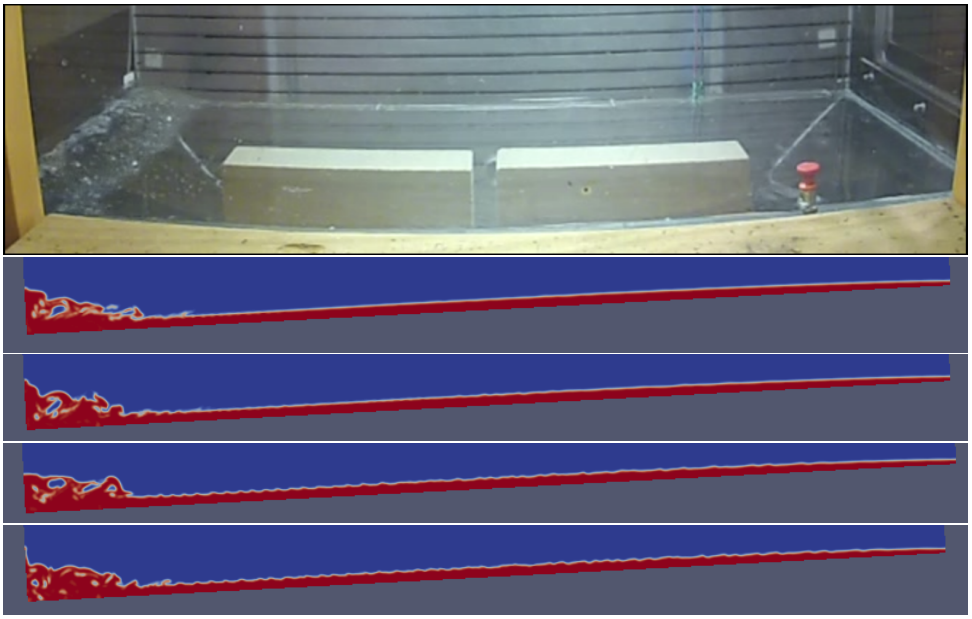

Figure D4: Images for tank test, S13, S14, S15 and S16 at t=2.7s

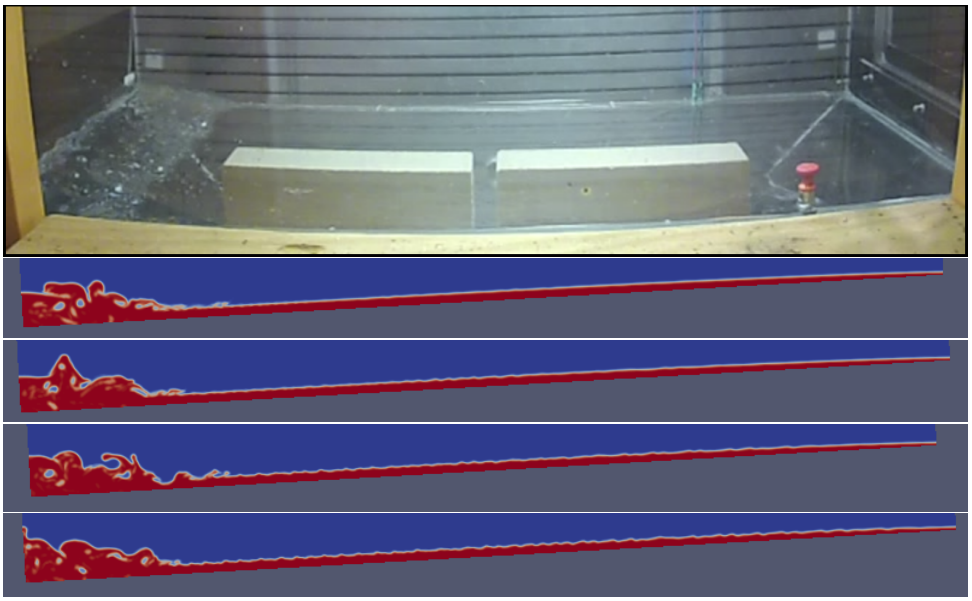

Figure D5: Images for tank test, S13, S14, S15 and S16 at t=2.85s

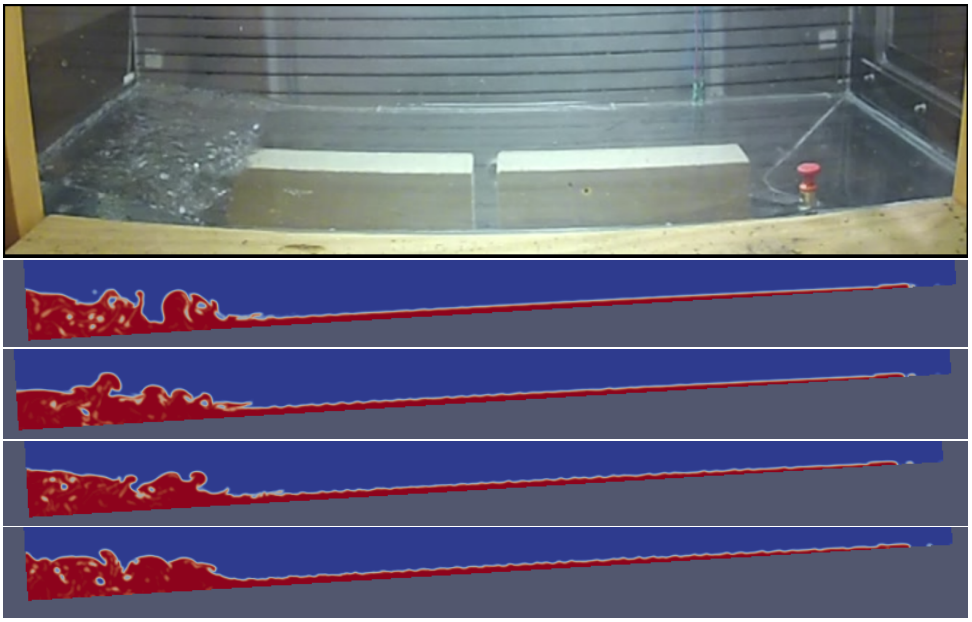

Figure D6: Images for tank test, S13, S14, S15 and S16 at t=3.15s

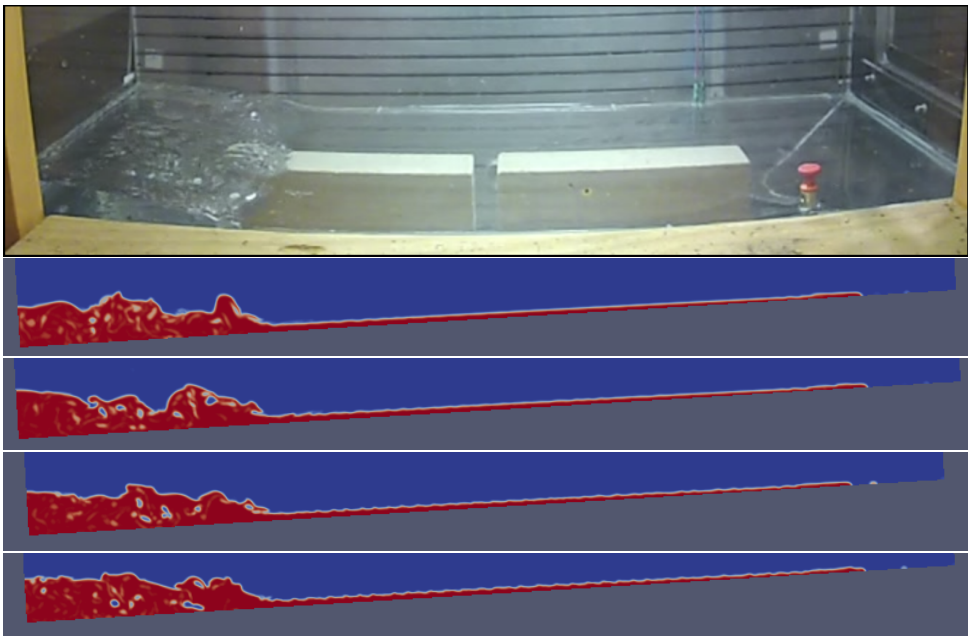

Figure D7: Images for tank test, S13, S14, S15 and S16 at t=3.3s

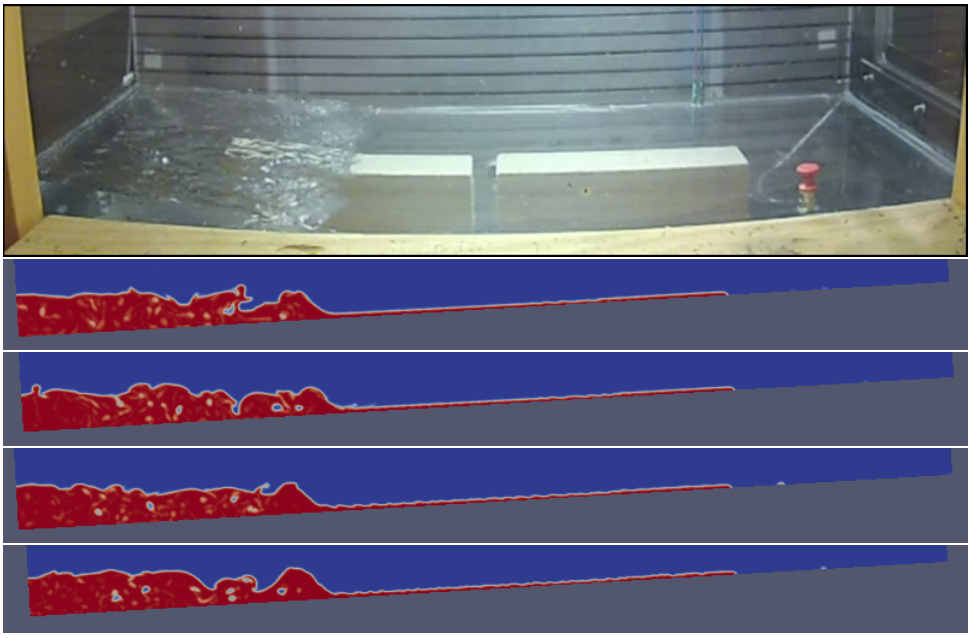

Figure D8: Images for tank test, S13, S14, S15 and S16 at t=3.6s

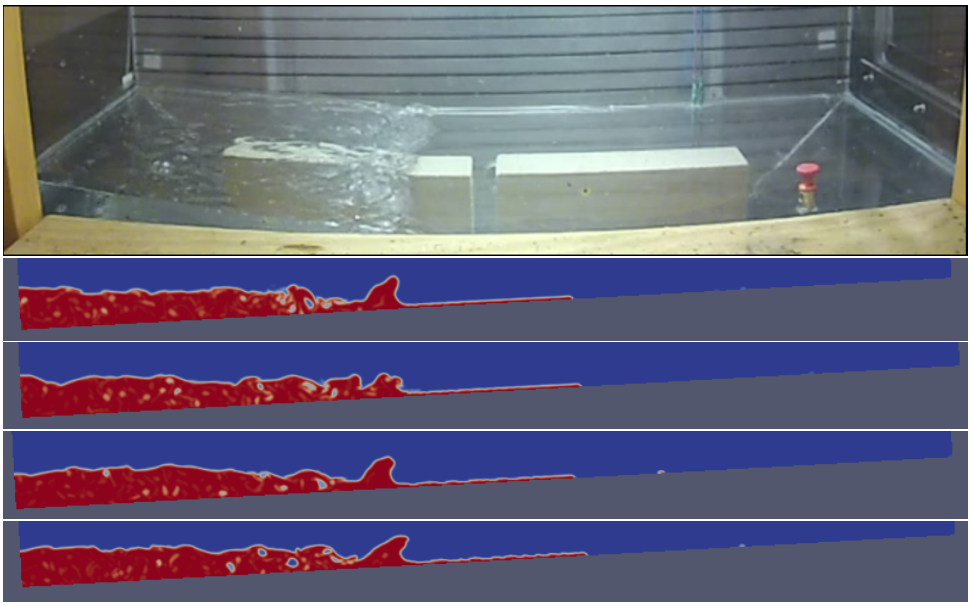

Figure D9: Images for tank test, S13, S14, S15 and S16 at t=3.9s

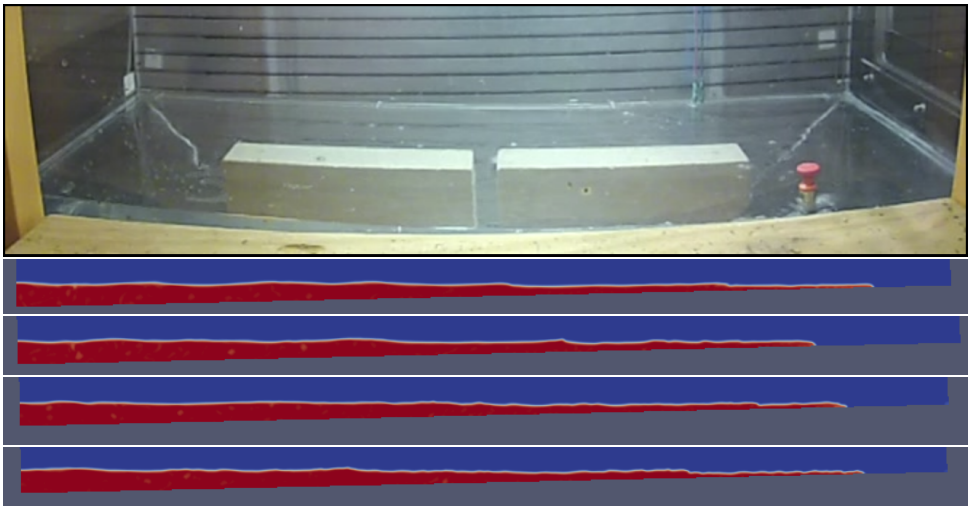

Figure D10: Images for tank test, S13, S14, S15 and S16 at t=5.4s